

# One-dimensional slow invariant manifolds for spatially homogenous reactive systems

Ashraf N. Al-Khateeb,<sup>1</sup> Joseph M. Powers,<sup>1,2,a)</sup> Samuel Paolucci,<sup>1</sup> Andrew J. Sommese,<sup>2</sup> Jeffrey A. Diller,<sup>2</sup> Jonathan D. Hauenstein,<sup>2</sup> and Joshua D. Mengers<sup>1</sup>

<sup>1</sup>*Department of Aerospace and Mechanical Engineering, University of Notre Dame, Notre Dame, Indiana 46556-5637, USA*

<sup>2</sup>*Department of Mathematics, University of Notre Dame, Notre Dame, Indiana 46556-4618, USA*

(Received 9 March 2009; accepted 17 June 2009; published online 14 July 2009)

A reactive system's slow dynamic behavior is approximated well by evolution on manifolds of dimension lower than that of the full composition space. This work addresses the construction of one-dimensional slow invariant manifolds for dynamical systems arising from modeling unsteady spatially homogeneous closed reactive systems. Additionally, the relation between the systems' slow dynamics, described by the constructed manifolds, and thermodynamics is clarified. It is shown that other than identifying the equilibrium state, traditional equilibrium thermodynamic potentials provide no guidance in constructing the systems' actual slow invariant manifolds. The construction technique is based on analyzing the composition space of the reactive system. The system's finite and infinite equilibria are calculated using a homotopy continuation method. The slow invariant manifolds are constructed by calculating attractive heteroclinic orbits which connect appropriate equilibria to the unique stable physical equilibrium point. Application of the method to several realistic reactive systems, including a detailed hydrogen-air kinetics model, reveals that constructing the actual slow invariant manifolds can be computationally efficient and algorithmically easy.

© 2009 American Institute of Physics. [DOI: [10.1063/1.3171613](https://doi.org/10.1063/1.3171613)]

## I. INTRODUCTION

Modeling physical problems of multiscale nature is a formidable task, even with modern computational capabilities. Typical examples are found in atmospheric chemistry,<sup>1</sup> biochemistry,<sup>2</sup> and combustion,<sup>3</sup> where a number of physical and chemical processes that occur at different scales exist. In simulation, the presence of a broad range of scales incurs a large computational cost.<sup>4</sup> In the case of combustion, this cost increases with the number of species and the number of reactions.<sup>5</sup> Also, as the range of time scales widens, solution verification becomes increasingly difficult. In the literature, numerous methods based on several approaches have been proposed to reduce the computational cost of simulating reactive systems described by detailed kinetics.<sup>6–23</sup> The main challenge for these methods is to simplify the model equations without significant loss of accuracy.

For spatially homogeneous reactive systems, reaction dynamics are described by a set of nonlinear coupled ordinary differential equations (ODEs). The solutions of this set of ODEs are represented by trajectories in the species composition space. Each trajectory represents the reactive system's evolution with time for a specific initial condition. After a short transient, the evolved trajectories seem to be attracted to a special trajectory and stay exponentially close to it until they reach equilibrium in infinite time.<sup>12</sup> The reactive system's slow modes are the only active ones on this special trajectory. This implies that the system's slow dynamics can be described by these manifolds which are of

smaller dimension than the full composition space dimension.<sup>17</sup> Thus, identifying this manifold for a reactive system makes it possible to reduce the computational cost by filtering the system's fast modes. Such an approach relies on identifying these manifolds within the species composition space which describes the slow dynamics of a reactive system.<sup>19–23</sup>

The dimension reduction approach can significantly reduce the computational cost of modeling the detailed kinetics of a reactive system.<sup>21</sup> This approach is based on representing the chemistry of a reactive system's variables in terms of the chemistry of a reduced number of variables. Within the dimension reduction approach, two major techniques exist. The first set of methods employs local linear time scale analysis to separate the system's modes into fast and slow, such as intrinsic low-dimensional manifolds (ILDMs),<sup>10</sup> computational singular perturbation (CSP),<sup>12–14</sup> and global quasilinearization (GQL).<sup>11</sup> The dynamics are segregated using chemical bases. These bases are generated *a priori* in the ILDM and GQL, while in the CSP they are estimated locally by iteration. Although ILDM is more efficient than CSP, it is less accurate.<sup>24,25</sup> Furthermore, the calculated manifolds using ILDM and GQL are not invariant.<sup>26</sup>

The second set of methods, which is the main subject of this work, employs a geometrical approach to describe the multiscale kinetics. Examples include the quasisteady state assumption,<sup>27</sup> iterative methods,<sup>15,16</sup> the Davis and Skodje method,<sup>17</sup> the minimal entropy production trajectory (MEPT) method,<sup>19,28</sup> the method of invariant manifold (MIM),<sup>20</sup> the rate-controlled constrained equilibrium (RCCE) method,<sup>29,30</sup> and the invariant constrained equilibrium edge preimage

<sup>a)</sup>Electronic mail: powers@nd.edu.

curve (ICE-PIC) method.<sup>21,31</sup> The Davis and Skodje method and the iterative methods are the most accurate among these approaches.<sup>32,33</sup> The Davis and Skodje method is based on a global composition space analysis of the full dynamics of a reactive system. However, such construction has been done only for small model systems.<sup>17,22</sup> The iterative methods are based on constructing the attractive invariant manifold from the system trajectories. Although these methods have a rapid rate of convergence, they require a sufficiently accurate guess to converge.<sup>17</sup> Also, these methods have been used only for small model systems.

The MEPT, MIM, RCCE, and ICE-PIC methods employ classical thermodynamics far from the equilibrium state to construct the attractive manifolds. While results from this class of methods may seem intuitive, they have not been fully compared to the more accurate iterative methods or Davis and Skodje method. Moreover, the MEPT approach relies on the concept of minimum entropy production.<sup>34</sup> The validity of this principle has been called into question in other fields, e.g., heat diffusion.<sup>35</sup>

The slow invariant manifold (SIM) for a reactive system is a subset of the species composition space. It describes the asymptotic structure of the invariant attracting reactive system's trajectories during their relaxation toward equilibrium. This work focuses on constructing only one-dimensional (1D) SIMs, although for each reactive system there are SIMs of different dimensions.

A heteroclinic orbit is defined as a trajectory that connects two critical points. A 1D SIM is defined here as a heteroclinic orbit that is locally attractive along the complete trajectory. A similar idea has been investigated before in literature.<sup>17,22,23</sup> With the exceptions of the iterative methods and the technique presented by Davis and Skodje, all previously discussed methods, and any other method based on them, only approximate the reactive systems' actual SIMs or parts of them.

The present paper offers the first construction of a SIM for a realistic detailed kinetics system. The main goal of this work is to identify a reactive system's actual 1D SIM. We confine our attention to isothermal systems, although extension to nonisothermal systems is straightforward. This paper is organized as follows. In Sec. II the mathematical foundation is presented for closed isothermal spatially homogenous reactive systems. Then, in Sec. III the proposed method to construct the actual 1D SIM is presented in a geometric frame. In Sec. IV, several test cases are introduced, and their actual 1D SIMs are constructed. Moreover, comparisons to other methods are conducted. Then, results for a hydrogen-air reactive system using detailed kinetics are presented, and lastly conclusions are stated.

## II. MATHEMATICAL BACKGROUND

In this section, a brief description of the governing equations is presented. The superscript (*o*) denotes evaluation at reference pressure, quantities with superscripts (\*) and (*e*) correspond, respectively, to the initial state and to the equilibrium state, and quantities with an overbar ( $\bar{\phantom{x}}$ ) denote the evaluation of these quantities on a molar basis.

## A. Model equations

We consider a closed, spatially homogenous, premixed reactive mixture of calorically imperfect ideal gases described by detailed mass-action kinetics. The mixture is confined in a volume  $V$  at temperature  $T$  and pressure  $p$ . This mixture consists of  $N$  species composed of  $L$  atomic elements which undergo  $J$  reversible reactions of the form

$$\sum_{i=1}^N \nu'_{ij} \chi_i = \sum_{i=1}^N \nu''_{ij} \chi_i, \quad j = 1, \dots, J. \quad (1)$$

Here,  $\chi_i$  is the chemical symbol of species  $i$ , and for the  $j$ th reaction,  $\nu'_{ij}$  and  $\nu''_{ij}$  are the stoichiometric coefficients of species  $i$ , denoting the number of moles of reactants and products, respectively. For such mixtures, the total mass ( $M$ ) remains constant throughout the reaction process, and for each reaction in the mechanism the mass of each element is conserved. Total mass and element mass balances are enforced by the following linear relations:

$$M = \sum_{i=1}^N \bar{M}_i n_i = \sum_{i=1}^N \bar{M}_i n_i^*, \quad (2a)$$

$$\sum_{i=1}^N \phi_{li} \nu_{ij} = 0, \quad l = 1, \dots, L, \quad j = 1, \dots, J, \quad (2b)$$

where  $\bar{M}_i$ ,  $n_i$ , and  $\phi_{li}$  are, respectively, the molecular mass of species  $i$ , the number of moles of species  $i$ , and the element index matrix, which provides the number of moles of element  $l$  in species  $i$ . Also,  $\nu_{ij} = \nu''_{ij} - \nu'_{ij}$  is the stoichiometric matrix, which gives the net stoichiometric coefficient for species  $i$  in reaction  $j$ . Equation (2b) demands that  $\nu_{ij}$  lie in the right null space of  $\phi_{li}$  and physically means that the mass and number of moles of each element is conserved in each reaction. In general,  $\phi_{li}$  and  $\nu_{ij}$  are nonsquare matrices of dimensions  $L \times N$  and  $N \times J$ , respectively. However,  $\phi_{li}$  is of full rank, while  $\nu_{ij}$  is of rank  $R \leq (N-L)$ ; commonly  $R = (N-L)$ . In this work, we focus on systems in which  $J \geq R$ . However, for less common systems in which  $J < R$ , our analysis can be easily modified.

The change in the number of moles of species  $i$  with time ( $t$ ) due to chemical reaction is described by the following system:<sup>36</sup>

$$\frac{dn_i}{dt} = V \sum_{j=1}^J \nu_{ij} r_j, \quad i = 1, \dots, N, \quad (3a)$$

$$n_i|_{t=0} = n_i^*, \quad i = 1, \dots, N, \quad (3b)$$

where

$$r_j = k_j \left( \prod_{i=1}^N \left( \frac{n_i}{V} \right)^{\nu'_{ij}} - \frac{1}{K_j^c} \prod_{i=1}^N \left( \frac{n_i}{V} \right)^{\nu''_{ij}} \right), \quad j = 1, \dots, J, \quad (4)$$

is the reaction rate given by the law of mass action. Here, for the  $j$ th reaction,  $k_j$  and  $K_j^c$  are, respectively, the Arrhenius kinetic rates given by

$$k_j = A_j T^{\beta_j} \exp\left(\frac{-\bar{E}_j}{\mathfrak{R}T}\right), \quad j = 1, \dots, J, \quad (5)$$

and the equilibrium constants given by

$$K_j^c = \left(\frac{p^o}{\mathfrak{R}T}\right)^{\sum_{i=1}^N \nu_{ij}} \exp\left(-\frac{\sum_{i=1}^N \bar{\mu}_i^o \nu_{ij}}{\mathfrak{R}T}\right), \quad j = 1, \dots, J. \quad (6)$$

In Eqs. (5) and (6),  $\bar{\mathfrak{R}} = 8.314 \times 10^7$  erg/mol/K is the universal gas constant, and for each reaction the quantities  $A_j$ ,  $\beta_j$ , and  $\bar{E}_j$  represent the collision frequency factor, the temperature-dependency exponent, and the activation energy, respectively. Also,  $\bar{\mu}_i^o$  are the chemical potentials given by

$$\bar{\mu}_i^o = \bar{M}_i(h_i - Ts_i^o), \quad i = 1, \dots, N. \quad (7)$$

Here,  $h_i$  and  $s_i^o$  are the specific enthalpy and the specific entropy of species  $i$ . For ideal gases,  $h_i$  and  $s_i^o$  are constant for a given  $T$ .

## B. Thermodynamic conditions

Adopting Dalton's law for ideal mixtures and considering a mixture of calorically imperfect ideal gases implies that the thermal state equation is

$$p = \frac{\bar{\mathfrak{R}}Tn}{V}, \quad (8a)$$

where

$$n = \sum_{i=1}^N n_i. \quad (8b)$$

Also, the mixture Gibbs free energy ( $G$ ) is given by the following relation:<sup>37</sup>

$$G = \sum_{i=1}^N n_i \bar{\mu}_i, \quad (9a)$$

where

$$\bar{\mu}_i = \bar{\mu}_i^o + \bar{\mathfrak{R}}T \ln\left(\frac{pX_i}{p^o}\right), \quad i = 1, \dots, N. \quad (9b)$$

Here,  $X_i = n_i/n$  is the mole fraction of species  $i$ . This thermodynamic property is of special interest. The minimum of  $G$  within the region of composition space with positive  $n_i$  corresponds to the reactive system's equilibrium state,<sup>38</sup> which is identified by the following relation:

$$\sum_{i=1}^N \nu_{ij} \bar{\mu}_i = 0, \quad j = 1, \dots, J. \quad (10)$$

Another thermodynamic property of interest is the mixture entropy ( $S$ ), which is defined as

$$S = \sum_{i=1}^N n_i \bar{s}_i. \quad (11a)$$

where

$$\bar{s}_i = \bar{M}_i s_i^o - \bar{\mathfrak{R}} \ln\left(\frac{pX_i}{p^o}\right). \quad (11b)$$

The differential change of  $S$  is postulated by the second law of thermodynamics,<sup>38</sup> although it is stated differently in nonequilibrium thermodynamics than in classical thermodynamics.<sup>37</sup> In nonequilibrium thermodynamics, the differential change of  $S$  is denoted as<sup>39</sup>

$$dS = d_e S + d_i S, \quad (12a)$$

in which  $d_e S$  is the change in entropy due to the system's exchange of matter and energy with its surroundings, and

$$d_i S = -\frac{1}{T} \sum_{i=1}^N \bar{\mu}_i dn_i, \quad (12b)$$

is the change in entropy due to irreversible processes within the system. Thus, an expression for the irreversibility production rate ( $\sigma$ ), also known as the entropy production rate, is introduced as<sup>34</sup>

$$\sigma = \frac{d_i S}{dt} = -\frac{1}{T} \sum_{i=1}^N \bar{\mu}_i \frac{dn_i}{dt}. \quad (13)$$

Similar to  $G$ ,  $\sigma$  is a convex function in composition space with a minimum at the reactive system's equilibrium point.

## C. Governing equations

The complete system, Eq. (3), defines an  $N$ -dimensional composition space. But, in any closed reactive system the total number of moles of each element is conserved. By multiplying both sides of Eq. (3a) by  $\phi_{li}$ , summing the result from  $i=1$  to  $N$ , employing Eq. (2b) to set the right side to zero, integrating the resulting homogeneous differential equation, and applying the initial condition, Eq. (3b), we obtain

$$\sum_{i=1}^N \phi_{li} n_i = \sum_{i=1}^N \phi_{li} n_i^*, \quad l = 1, \dots, L. \quad (14)$$

Generally, Eq. (14) is an underconstrained linear system of  $L$  equations for the  $N$  values of  $n_i$ .<sup>40</sup> This implies it has solutions of the following form:

$$n_i = n_i^* + \mathbf{M} \left( \sum_{k=1}^R \mathcal{D}_{ik} z_k \right), \quad i = 1, \dots, N. \quad (15)$$

Here,  $z_k = n_k/M$ ,  $k=1, \dots, R$ , is a reduced composition variable which physically represents the number of moles of species  $k$  per total mass and  $\mathcal{D}_{ik}$  is a dimensionless constant matrix of size  $N \times R$  and has a full rank  $R$ . Each column vector of  $\mathcal{D}_{ik}$  is linearly independent of the remaining column vectors. However,  $\mathcal{D}_{ik}$  is not unique; it can be constructed in several ways. In this work,  $\mathcal{D}_{ik}$  is constructed using the following procedure. First, a row-echelon form of the  $\nu_{ij}$  matrix is obtained by performing a series of row operations on Eq. (3a). The number of nonzero rows in the row-echelon form of  $\nu_{ij}$  is the rank of  $\nu_{ij}$  and  $\mathcal{D}_{ik}$ , since  $\nu_{ij}$  and  $\mathcal{D}_{ik}$  span the same column space. We use elementary row operations to identify the  $N \times N$  lower triangular matrix ( $\mathbf{L}$ ),

which, when matrix multiplied with Eq. (3a) yields  $\mathbf{L} \cdot d\mathbf{n}/dt = V\mathbf{U} \cdot \mathbf{r}$ , where  $\mathbf{U} = \mathbf{L} \cdot \boldsymbol{\nu}$  is an upper triangular matrix of dimension  $N \times R$ . This nonunique matrix describes the system's linear constraints, which are obtained by integrating the  $N-R$  homogenous ODEs that are obtained as a result of reduction to the row-echelon form. Then, the  $\mathcal{D}_{ik}$  matrix is constructed such that the first  $R$  row vectors of it are set in the reduced row-echelon form, while the other row vectors are obtained using  $\mathbf{L}$  to reflect the system's constraints. A detailed example will be given later to illustrate the construction of  $\mathcal{D}_{ik}$  for a realistic reactive system.

Equation (15) allows the  $N$  species to be represented in terms of  $R$  dependent variables. First, take the time derivative of Eq. (15) to get

$$\frac{dn_i}{dt} = M \left( \sum_{k=1}^R \mathcal{D}_{ik} \frac{dz_k}{dt} \right), \quad i = 1, \dots, N. \quad (16a)$$

Now, by substituting Eq. (3a) into Eq. (16a), we obtain

$$\frac{V}{M} \dot{\omega}_i = \left( \sum_{k=1}^R \mathcal{D}_{ik} \frac{dz_k}{dt} \right), \quad i = 1, \dots, N, \quad (16b)$$

where

$$\dot{\omega}_i = \sum_{j=1}^J \nu_{ij} r_j, \quad i = 1, \dots, N, \quad (16c)$$

is the molar production rate per unit volume of species  $i$ . In Gibbs notation, Eq. (16b) is written as

$$\frac{V}{M} \dot{\boldsymbol{\omega}} = \mathcal{D} \cdot \frac{d\mathbf{z}}{dt}, \quad \mathbf{z} \in \mathbb{R}^R, \quad \dot{\boldsymbol{\omega}} \in \mathbb{R}^N. \quad (16d)$$

Since  $\mathcal{D}$  is nonsquare, we take the matrix product of both sides of Eq. (16d) with  $\mathcal{D}^T$  to obtain

$$\frac{V}{M} \mathcal{D}^T \cdot \dot{\boldsymbol{\omega}} = \mathcal{D}^T \cdot \mathcal{D} \cdot \frac{d\mathbf{z}}{dt}, \quad \mathbf{z} \in \mathbb{R}^R, \quad \dot{\boldsymbol{\omega}} \in \mathbb{R}^N. \quad (16e)$$

Then, to remove  $\mathcal{D}$  from the right hand side of Eq. (16e), we take the matrix product of both sides by  $(\mathcal{D}^T \cdot \mathcal{D})^{-1}$ . Consequently, the rate of evolution of the species in the reactive mixture is governed by

$$\frac{dz_k}{dt} = \dot{w}_k, \quad k = 1, \dots, R, \quad (17a)$$

$$z_k|_{t=0} = z_k^*, \quad k = 1, \dots, R, \quad (17b)$$

where

$$\dot{w}_k = \frac{1}{\rho} \sum_{j=1}^R \left[ \left( \sum_{i=1}^N \mathcal{D}_{ik} \mathcal{D}_{ij} \right)^{-1} \left( \sum_{i=1}^N \mathcal{D}_{ij} \dot{\omega}_i \right) \right], \quad k = 1, \dots, R, \quad (18)$$

is the molar production rate of species  $k$  in the reduced composition space and  $\rho = M/V$  is the mixture mass density. So, the reactive system's solutions, represented as trajectories, move within the reduced composition space  $\mathbb{R}^R$ , where  $\mathbb{R}^R \subset \mathbb{R}^N$ .

### III. METHODOLOGY

From a geometric point of view, the species specific moles  $\mathbf{z}$  correspond to a vector in the Euclidian composition space  $\mathbb{R}^R$ . This vector is given by the following relation:

$$\mathbf{z} = \mathcal{L}(\mathbf{n}) \mid \mathcal{L}: (\mathbb{R}^N \rightarrow \mathbb{R}^R), \quad (19)$$

where

$$\mathcal{L}(\mathbf{n}) = \frac{1}{M} (\mathcal{D}^T \cdot \mathcal{D})^{-1} \cdot \mathcal{D}^T \cdot (\mathbf{n} - \mathbf{n}^*) \quad (20)$$

is a linear operator that accounts for all the system's linear constraints. The evolution of  $\mathbf{z}$  in time is described as an autonomous dynamical system of the standard form,

$$\frac{d\mathbf{z}}{dt} = \mathbf{f}(\mathbf{z}), \quad \mathbf{z} \in \mathbb{R}^R, \quad (21)$$

where  $\mathbf{f}$  is a set of  $R$  nonlinear coupled algebraic functions. For our isothermal system, these functions are polynomials of degree  $d$  connected with a given reaction mechanism.

The construction method of the SIM is based on identifying all the equilibria of the dynamical system that describes the species evolution, Eq. (21). In general, the set of equilibria of such functions is complex,

$$\mathbf{z}^e \in \mathbb{C}^R \mid \mathbf{f}(\mathbf{z}^e) = \mathbf{0}. \quad (22)$$

Also, as demonstrated by Perko,<sup>41</sup> the set of equilibria  $\mathbf{z}^e$  contains finite equilibria and equilibria located at infinity. Both classes of equilibria will be of interest. Furthermore, the equilibria can be positive dimensional continua; i.e., high-dimensional equilibria. Such equilibria have dimension larger than zero; 1D equilibria are curves, two-dimensional (2D) equilibria are surfaces, three-dimensional (3D) equilibria are volumes, etc.<sup>42,43</sup> Here, BERTINI,<sup>44</sup> a code based on homotopy continuation, is used to obtain the system's equilibria to any desired accuracy. Then, the equilibria are connected via trajectories obtained by numerical integration of the species evolution equations using any computationally inexpensive scheme; here we use the fourth-order Runge-Kutta scheme. Finally, we are able to identify the 1D SIM that describes the asymptotic structure of the invariant attracting trajectories.

In this work, all calculations have been performed to 100 significant digits. However, all the listed results have been rounded to three significant digits. Integer values indicate that the reported numbers are exact. The thermodynamic properties are obtained from the public domain edition of the CHEMKIN package.<sup>45</sup> Subsequently, the property values are treated as having infinite precision. For the results presented in Sec. IV, the computational time to construct any 1D SIM is approximately 15 s on a MacBookPro 2.16 GHz machine, including the identification of the equilibria. However, the computational time to construct the 1D SIM presented in Sec. V is approximately 60 s on the same machine.

#### A. Equilibria: BERTINI

BERTINI is a software package designed to compute the solutions of polynomial systems over  $\mathbb{C}$  using homotopy

continuation. Polynomial systems that arise from chemical reactions are often poorly scaled which can lead to numerical difficulties when computing the solutions. When BERTINI is used to solve polynomial systems as discussed in this work, the polynomial systems are first rescaled using SCLGEN.<sup>46</sup> SCLGEN is an algorithm that uses both a change of variables and equation scaling to rescale the given polynomial system into one which has coefficients of reduced variability and centered about unity, i.e., a rescaling of the equations to reduce the magnitude differences between the coefficients of the equations. For example, if  $f_1(z_1, \dots, z_R), \dots, f_R(z_1, \dots, z_R)$  are polynomials, SCLGEN computes real constants  $\alpha_1, \dots, \alpha_R$  and  $\beta_1, \dots, \beta_R$  to define the rescaled system  $g_1(x_1, \dots, x_R), \dots, g_R(x_1, \dots, x_R)$  by

$$\mathbf{g}(\mathbf{x}) = \boldsymbol{\beta} \cdot \mathbf{f}(\boldsymbol{\alpha} \cdot \mathbf{z}), \quad \{\mathbf{g}, \mathbf{f}, \mathbf{z}, \boldsymbol{\alpha}, \boldsymbol{\beta}\} \in \mathbb{R}^R.$$

Reference 42 provides a detailed description of using homotopy continuation to describe all solutions to a given polynomial system.

## B. Finite equilibria

To obtain the dynamical system's finite equilibria, we find all the  $\mathbf{z}^e$  that satisfy  $\mathbf{f}(\mathbf{z}^e) = 0$ . One of these finite equilibria is the reactive system's physical equilibrium point. This critical point is of special interest; it represents the minimum of  $G$ . Moreover, it is the only critical point located inside the physically accessible domain (S),<sup>40</sup> which is defined as a subspace within the reduced composition space where all the species are positive semidefinite and finite,

$$S \subset \mathbb{R}^R \mid \mathbf{n} \geq 0. \quad (23)$$

The rest of the finite equilibria are located outside S; they are nonphysical since at least one of the species mole numbers is negative,  $n_i < 0$ .

Next, the dynamic behavior of the system within the neighborhood of each finite equilibrium is investigated by employing standard linearization techniques. For a hyperbolic equilibrium,<sup>41</sup> the Hartman–Grobman theorem is used to reveal its dynamical character. For a nonhyperbolic equilibrium, the Hartman–Grobman theorem is not applicable, so the normal form theory<sup>41,47</sup> is utilized to reveal the dynamical character of the equilibrium. The Hartman–Grobman theorem and the normal form theory are briefly reviewed in the Appendix. First, we linearize the system in the neighborhood of each equilibrium. We start by defining the perturbation from the equilibrium as  $\mathbf{z}' = \mathbf{z} - \mathbf{z}^e$ . The dynamics can be described locally as

$$\frac{d\mathbf{z}'}{dt} = \mathbf{J}^e \cdot \mathbf{z}' + \mathcal{O}(\mathbf{z}'^2). \quad (24a)$$

Here,

$$\mathbf{J}^e = \left. \frac{\partial \mathbf{f}}{\partial \mathbf{z}} \right|_{\mathbf{z}=\mathbf{z}^e} \quad (24b)$$

is the constant Jacobian matrix evaluated at an equilibrium. The stability of each equilibrium is determined by examining the eigenvalue spectrum  $\lambda_i$  of  $\mathbf{J}^e$  and the corresponding eigenvectors  $\mathbf{v}_i$ . The local time scales over which the dy-

namical system, Eq. (21), evolves are given by the reciprocal of the real part of the system's eigenvalues,  $1/|\text{Re}(\lambda_i)|$ .

In general, the eigenvalues are complex, where the reciprocal of the real parts provides the scales of the amplitude growth, and the reciprocal of the imaginary parts represents the period of oscillations. The physical equilibrium point must be a stable node;<sup>48</sup> i.e., all the eigenvalues of  $\mathbf{J}^e$  are real and negative. Furthermore, the ratio between the largest and smallest time scales identifies the system's stiffness. In addition, the eigenvector associated with the least negative eigenvalue represents the system's slowest mode or direction in composition space along which the trajectories approach the equilibrium. Similarly, the eigenvector associated with the largest eigenvalue represents the system's fastest mode.

## C. Infinite equilibria

To identify the dynamical system's infinite equilibria, the projective space technique is employed.<sup>42,46,49</sup> This technique maps the critical points at infinity into the finite domain where they can be easily computed. The projective space mapping, given here in its simplest form for pedagogical purposes, consists of the following one-to-one transformation:

$$Z_k = \frac{1}{z_k}, \quad k \in \{1, \dots, R\}, \quad (25a)$$

$$Z_i = \frac{z_i}{z_k}, \quad i \neq k, \quad i = 1, \dots, R, \quad (25b)$$

where  $z_k$  is any arbitrarily selected dependent variable and  $\mathbf{Z}$  are the state variables in the projective space. As a result of employing this transformation, the infinite equilibria are mapped onto the line  $Z_k = 0$ . In certain cases there is a degeneracy in this transformation. We omit further details, but this is overcome in practice by employing the more robust transformation,

$$Z_k = \frac{1}{\sum_{j=1}^R a_j z_j}, \quad k \in \{1, \dots, R\}, \quad (26a)$$

$$Z_i = \frac{z_i}{\sum_{j=1}^R a_j z_j}, \quad i \neq k, \quad i = 1, \dots, R, \quad (26b)$$

where we take  $a_j \in [0, 1]$  to be a set of random numbers, such that  $\sum_{j=1}^R a_j = 1$ .

The projective space technique has the disadvantage of introducing a singularity in the dynamical system. To overcome this difficulty, we define a transformed independent variable  $\tau$  in the projective space which is related to  $t$  in the original space as follows:

$$\frac{dt}{d\tau} = (Z_k)^{d-1}, \quad (27)$$

where we recall that  $d$  is the maximum degree of the polynomials in  $\mathbf{f}$ . By employing this mapping, the original dynamical system, Eq. (21), is recast in the projective space in the following form:

$$\begin{aligned}
 \frac{d\mathbf{Z}}{d\tau} &= \frac{d}{d\tau} \begin{pmatrix} Z_0 \\ Z_1 \\ \vdots \\ Z_{k-1} \\ Z_k \\ Z_{k+1} \\ \vdots \\ Z_R \end{pmatrix} \\
 &= \mathbf{Z}_k^d \cdot \begin{pmatrix} Z_k^{-1} \\ f_1(Z_1, \dots, Z_R) - Z_1 f_k(Z_1, \dots, Z_R) \\ \vdots \\ f_{k-1}(Z_1, \dots, Z_R) - Z_{k-1} f_k(Z_1, \dots, Z_R) \\ - Z_k f_k(Z_1, \dots, Z_R) \\ f_{k+1}(Z_1, \dots, Z_R) - Z_{k+1} f_k(Z_1, \dots, Z_R) \\ \vdots \\ f_R(Z_1, \dots, Z_R) - Z_R f_k(Z_1, \dots, Z_R) \end{pmatrix} \\
 &= \mathbf{F}(\mathbf{Z}), \tag{28}
 \end{aligned}$$

where we denote  $Z_0 = t$ . The finite equilibria satisfying  $\mathbf{F}(\mathbf{Z}^e) = \mathbf{0}$  of the resulting dynamical system, Eq. (28), represent the infinite equilibria of the original dynamical system, Eq. (21). We note here that  $\mathbf{Z} \in \mathbb{R}^{R+1}$ , although the value of  $Z_0^e$  is irrelevant.

#### D. Construction method

Here, the procedure for constructing the closed spatially homogenous reactive system's 1D SIM is presented. In this, the following conjecture has been found to be useful. At this stage we have no formal proof for it.

*Conjecture: Only the system's isolated nonphysical real finite and infinite equilibria are relevant to the construction of a 1D SIM connecting to the physical equilibrium. Furthermore, among these nonphysical equilibria, only those with one unstable eigenvector direction can be candidate members of the 1D SIM.*

As a consequence of the first part of the conjecture, the high-dimensional equilibria and the complex equilibria are not relevant to this study. Furthermore, as a consequence of the second part of the conjecture, the real critical points with the following dynamical character are excluded: sinks, sources, saddles with more than one positive eigenvalue, and nonhyperbolic equilibria with more than one positive eigenvalue.

The system's finite and infinite equilibria that satisfy our conjecture will be called candidate equilibria. Starting from each one of these equilibria, a heteroclinic orbit is generated tangent to its unstable direction. Only heteroclinic orbits that connect to the physical equilibrium are relevant to the construction of the 1D SIM. In general, the 1D SIM consists of at most two branches. Among the heteroclinic orbits, two such orbits represent the branches of the system's 1D SIM. These orbits can be identified since they are the only ones that approach the physical equilibrium point tangent to its slowest mode, and they are attractive.

First, the candidate points are categorized based on their location; the first category contains the finite candidate points, and the second category contains the candidate points located at infinity. Within each category the candidate points are ordered based on the magnitude of their unstable modes, i.e., positive eigenvalue. In each category, the first candidate point is taken as the one with the least positive eigenvalue, i.e., slowest time scale.

Next, we start the process of SIM construction by generating a heteroclinic orbit from the first candidate point in the first category; the finite candidate point with the least positive eigenvalue. To generate such an orbit, Eq. (21) is integrated in the direction of the eigenvector associated with the positive eigenvalue pointing toward the reactive system's physical equilibrium. Then, we check whether the generated orbit approaches the physical equilibrium point in the direction of its slowest mode, i.e., the eigenvector associated with the least negative eigenvalue at the physical equilibrium point. Subsequently, if the physical equilibrium is not located at the origin, another orbit is generated starting from the finite candidate point with the second lowest positive eigenvalue. If both of these orbits approach the physical equilibrium point in the direction of its slowest mode, then these two orbits correspond to the SIMs' two branches. Otherwise, we generate a new heteroclinic orbit from the finite candidate point with the third lowest eigenvalue, and so on. After using all finite candidate points, we follow the same procedure using the infinite candidate points. This procedure halts as soon as we construct two heteroclinic orbits that approach the physical equilibrium point in the direction of its slowest mode.

Finally, the attractiveness of the constructed 1D SIM is examined locally along the complete manifold. Here, in addition to visual examination, we pose the following criteria to hold along each branch of the 1D SIM. The eigenvalues  $\lambda_i$  of  $\mathbf{J}$  are computed locally along the heteroclinic orbit. Call  $\lambda_1$  the largest eigenvalue. Then we require that for  $i > 1$ ,

$$\lambda_i < 0 \quad \text{and} \quad \mathbf{S} \equiv \frac{|\lambda_1|}{|\lambda_i|} < 1. \tag{29}$$

The constraints ensure that the composition field contracts along the 1D SIM. Note that these criteria are more restrictive than the requirement for a contraction mapping, i.e.,  $\sum_{i=1}^R \lambda_i < 0$ . Furthermore, the criteria preclude the SIM from emanating from a source.

To summarize, we take the 1D SIM to consist of at most two heteroclinic orbits that are locally attractive along their complete trajectories.

#### IV. MODEL PROBLEMS

In this section, we illustrate our strategy for constructing a 1D SIM using three problems. The first problem is a simple but realistic reactive system. The other two systems have been used in the literature as prototypes for illustrating alternate techniques of constructing SIMs.

TABLE I. Zel'dovich mechanism of nitric acid formation. The species are NO, N, O, O<sub>2</sub>, and N<sub>2</sub>.

$j$	Reaction	$A_j$ [cm <sup>3</sup> /(mol s K <sup><math>\beta_j</math></sup> )]	$\beta_j$	$\bar{E}_j$ [cal/mol]
1	N+O <sub>2</sub> ⇌NO+O	5.841 × 10 <sup>9</sup>	1.01	6195.6
2	N+NO⇌N <sub>2</sub> +O	21.077 × 10 <sup>12</sup>	0.00	0.0

### A. Zel'dovich mechanism

A common reaction kinetics model is the Zel'dovich mechanism of nitric oxide formation.<sup>27</sup> This mechanism consists of  $N=5$  species,  $L=2$  elements, and  $J=2$  reversible reactions. Kinetic data are adopted from Baulch *et al.*,<sup>50</sup> see Table I. A special case in which the system is isochoric will be considered, and the assigned mixture temperature and volume are  $T=4000$  K and  $V=10^3$  cm<sup>3</sup>, respectively. For convenience, the assigned initial number of moles of each species is  $\mathbf{n}^*=10^{-3}$  mol.

Here,  $i=\{1,2,3,4,5\}$  correspond to the species {NO,N,O,O<sub>2</sub>,N<sub>2</sub>}, and  $l=\{1,2\}$  correspond to the elements {N,O}, respectively. For this system  $\phi$  has dimension  $2 \times 5$ ,

$$\phi = \begin{pmatrix} 1 & 1 & 0 & 0 & 2 \\ 1 & 0 & 1 & 2 & 0 \end{pmatrix},$$

and  $\nu$  has dimension  $5 \times 2$ ,

$$\nu = \begin{pmatrix} 1 & -1 \\ -1 & -1 \\ 1 & 1 \\ -1 & 0 \\ 0 & 1 \end{pmatrix}.$$

For the constraint of element conservation for each reaction, Eq. (2b), we have

$$\phi \cdot \nu = \begin{pmatrix} 0 & 0 \\ 0 & 0 \end{pmatrix}.$$

Thus, there are two element constraints in this model.

We start by formulating the set of ODEs that describes this kinetic model. Following Eq. (3a), we get

$$\frac{d}{dt} \begin{pmatrix} n_1 \\ n_2 \\ n_3 \\ n_4 \\ n_5 \end{pmatrix} = V \begin{pmatrix} 1 & -1 \\ -1 & -1 \\ 1 & 1 \\ -1 & 0 \\ 0 & 1 \end{pmatrix} \begin{pmatrix} r_1 \\ r_2 \end{pmatrix}, \quad (30a)$$

where, from Eq. (4),

$$r_1 = \frac{A_1 T^{\beta_1}}{V^2} \exp\left(\frac{-\bar{E}_1}{\mathfrak{R}T}\right) \left(n_2 n_4 - \frac{n_1 n_3}{K_1^c}\right),$$

$$r_2 = \frac{A_2 T^{\beta_2}}{V^2} \exp\left(\frac{-\bar{E}_2}{\mathfrak{R}T}\right) \left(n_2 n_1 - \frac{n_5 n_3}{K_2^c}\right).$$

Now, Eq. (30a) defines a real  $\mathbb{R}^N$  composition space. To reduce the dimension of this composition space, we construct the matrix  $\mathfrak{D}$ . First, we perform a series of row operations on Eq. (30a) to find all of the system's linear constraints; i.e., we generate the row-echelon form of  $\nu$ ,

$$\begin{pmatrix} 1 & 0 & 0 & 0 & 0 \\ 1 & 1 & 0 & 0 & 0 \\ 0 & 1 & 1 & 0 & 0 \\ \frac{1}{2} & -\frac{1}{2} & 0 & 1 & 0 \\ \frac{1}{2} & \frac{1}{2} & 0 & 0 & 1 \end{pmatrix} \frac{d}{dt} \begin{pmatrix} n_1 \\ n_2 \\ n_3 \\ n_4 \\ n_5 \end{pmatrix} = V \begin{pmatrix} 1 & -1 \\ 0 & -2 \\ 0 & 0 \\ 0 & 0 \\ 0 & 0 \end{pmatrix} \begin{pmatrix} r_1 \\ r_2 \end{pmatrix}, \quad (30b)$$

or in Gibbs notation,

$$\mathbf{L} \cdot \frac{d\mathbf{n}}{dt} = V(\mathbf{U} \cdot \mathbf{r}).$$

We note that the rank of  $\nu$  is  $R=2$  which corresponds to the number of the nonzero rows of  $\mathbf{U}=\mathbf{L} \cdot \nu$ .

In Eq. (30b) the last three equations are homogenous, so this model contains three linear constraints. Moreover, it implies that the behavior of  $\mathbf{n}$  as a function of time is described by the evolution of only two variables:  $n_1$  and  $n_2$ . The remaining variables,  $\{n_3, n_4, n_5\}$ , can be expressed in terms of  $n_1$  and  $n_2$ . These expressions are obtained by integrating the three homogenous equations in the system to obtain

$$n_2 + n_3 = c_1, \quad (31a)$$

$$\frac{1}{2}n_1 - \frac{1}{2}n_2 + n_4 = c_2, \quad (31b)$$

$$\frac{1}{2}n_1 + \frac{1}{2}n_2 + n_5 = c_3, \quad (31c)$$

where  $c_1$ ,  $c_2$ , and  $c_3$  are constants that are determined from  $\mathbf{n}^*$ . Further elementary row operations on Eqs. (31a)–(31c) reveal the following set:

$$n_1 + n_3 + 2n_4 = c_1 + 2c_2 = n_1^* + n_3^* + 2n_4^*, \quad (32a)$$

$$n_1 + n_2 + 2n_5 = 2c_3 = n_1^* + n_2^* + 2n_5^*, \quad (32b)$$

$$\sum_{i=1}^N n_i = c_1 + c_2 + c_3 = \sum_{i=1}^N n_i^*. \quad (32c)$$

Equations (32a) and (32b) indicate that the total number of moles of elemental oxygen and nitrogen are conserved. Equation (32c) states that the total number of molecules is constant. This last constraint is a consequence of including only bimolecular reactions in this kinetic model.

Now, by including the dependent variables, Eqs. (31a)–(31c) can be rearranged to obtain

$$\begin{pmatrix} n_1 \\ n_2 \\ n_3 \\ n_4 \\ n_5 \end{pmatrix} = \begin{pmatrix} 0 \\ 0 \\ c_1 \\ c_2 \\ c_3 \end{pmatrix} + \begin{pmatrix} 1 & 0 \\ 0 & 1 \\ 0 & -1 \\ -\frac{1}{2} & \frac{1}{2} \\ -\frac{1}{2} & -\frac{1}{2} \end{pmatrix} \begin{pmatrix} n_1 \\ n_2 \end{pmatrix}, \quad (33a)$$

and by introducing the reduced composition space variables as  $z_k = (n_k - n_k^*)/M$ ,  $k=1,2$ , we get

$$\begin{pmatrix} n_1 \\ n_2 \\ n_3 \\ n_4 \\ n_5 \end{pmatrix} = \begin{pmatrix} n_1^* \\ n_2^* \\ c_1 - n_2^* \\ c_2 - \frac{1}{2}n_1^* + \frac{1}{2}n_2^* \\ c_3 - \frac{1}{2}n_1^* - \frac{1}{2}n_2^* \end{pmatrix} + M \begin{pmatrix} 1 & 0 \\ 0 & 1 \\ 0 & -1 \\ -\frac{1}{2} & \frac{1}{2} \\ -\frac{1}{2} & -\frac{1}{2} \end{pmatrix} \begin{pmatrix} z_1 \\ z_2 \end{pmatrix}. \quad (33b)$$

Using Eqs. (32a)–(32c), this system can be rewritten as

$$\mathbf{n} = \begin{pmatrix} n_1 \\ n_2 \\ n_3 \\ n_4 \\ n_5 \end{pmatrix} = \begin{pmatrix} n_1^* \\ n_2^* \\ n_3^* \\ n_4^* \\ n_5^* \end{pmatrix} + M \begin{pmatrix} 1 & 0 \\ 0 & 1 \\ 0 & -1 \\ -\frac{1}{2} & \frac{1}{2} \\ -\frac{1}{2} & -\frac{1}{2} \end{pmatrix} \begin{pmatrix} z_1 \\ z_2 \end{pmatrix} \\ = \mathbf{n}^* + M\mathcal{D} \cdot \mathbf{z}. \quad (33c)$$

As we can see, this model problem is now described in the  $R=2$  dimensional reactive composition space. Using Eqs. (17a) and (18), the nonlinear ODE that describes the reactive system evolution is

$$\frac{d\mathbf{z}}{dt} = \mathbf{f}(\mathbf{z}) = \dot{\mathbf{w}}, \quad (34a)$$

where

$$\dot{\mathbf{w}} = \frac{-1}{\rho} \begin{pmatrix} r_2 - r_1 \\ r_1 + r_2 \end{pmatrix}. \quad (34b)$$

The mixture total mass is calculated using Eq. (2a),  $M = 1.20 \times 10^{-1}$  g. So, the mixture density is  $\rho = 1.20 \times 10^{-4}$  g/cm<sup>3</sup>. Explicitly, the evolution of the system is

$$\frac{dz_1}{dt} = 2.51 \times 10^2 + 1.16 \times 10^7 z_2 + 6.99 \times 10^8 z_2^2 - 9.98 \times 10^4 z_1 - 3.22 \times 10^9 z_2 z_1, \quad (35a)$$

$$\frac{dz_2}{dt} = 2.51 \times 10^2 - 1.17 \times 10^7 z_2 - 6.98 \times 10^8 z_2^2 + 8.47 \times 10^4 z_1 - 1.84 \times 10^9 z_2 z_1, \quad (35b)$$

where we note that the maximum degree of Eq. (35) is  $d=2$ .

### 1. Finite equilibria

The procedure described in Sec. III B is used to find the finite equilibria of the autonomous dynamical system, Eq. (34a), which describes the evolution of  $\mathbf{z}$ . By equilibrating the left hand side of Eq. (35) and using BERTINI to find all the  $\mathbf{z}^e$  that satisfy  $\mathbf{f}(\mathbf{z}^e) = 0$ , we find the following finite equilibria:

$$R_1 \equiv (\mathbf{z}^e) = (-1.78 \times 10^{-5}, -1.67 \times 10^{-2}) \text{ mol/g},$$

$$R_2 \equiv (\mathbf{z}^e) = (-4.20 \times 10^{-3}, -2.66 \times 10^{-5}) \text{ mol/g},$$

$$R_3 \equiv (\mathbf{z}^e) = (3.05 \times 10^{-3}, 2.94 \times 10^{-5}) \text{ mol/g}.$$

Here, all the finite equilibria are real isolated critical points. The rest of the species are obtained from Eq. (33c),

$$R_1 \equiv (\mathbf{n}^e) = (-2.14 \times 10^{-6}, -2.00 \times 10^{-3}, 4.00 \times 10^{-3}, 1.70 \times 10^{-8}, 3.00 \times 10^{-3}) \text{ mol},$$

$$R_2 \equiv (\mathbf{n}^e) = (-5.04 \times 10^{-4}, -3.20 \times 10^{-6}, 2.00 \times 10^{-3}, 1.25 \times 10^{-3}, 2.25 \times 10^{-3}) \text{ mol},$$

$$R_3 \equiv (\mathbf{n}^e) = (3.66 \times 10^{-4}, 3.53 \times 10^{-6}, 2.00 \times 10^{-3}, 8.19 \times 10^{-4}, 1.82 \times 10^{-3}) \text{ mol}.$$

It is clear that  $R_1$  and  $R_2$  are nonphysical equilibria, while  $R_3$  is a physical root that satisfies Eq. (23);  $R_3$  is the reactive system's unique physical equilibrium point.

To investigate the dynamical character of each critical point, first Eq. (35) is linearized to find  $\mathbf{J}^e$ . Following Eq. (24b) we obtain

$$\mathbf{J}^e = \begin{pmatrix} -9.98 \times 10^4 - 3.22 \times 10^9 z_2^e & 1.16 \times 10^7 + 1.40 \times 10^9 z_2^e - 3.22 \times 10^9 z_1^e \\ 8.47 \times 10^4 - 1.84 \times 10^9 z_2^e & -1.17 \times 10^7 - 1.40 \times 10^9 z_2^e - 1.84 \times 10^9 z_1^e \end{pmatrix}. \quad (36)$$

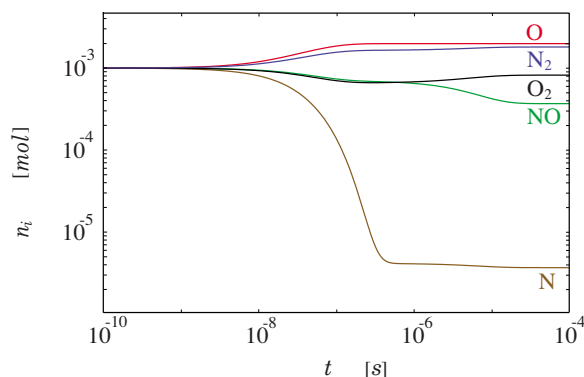


FIG. 1. The time evolution of species for the Zel'dovich model problem.

By substituting  $R_1$ ,  $R_2$ , and  $R_3$  into  $\mathbf{J}^e$ , linear analysis in the neighborhood of each critical point reveals that  $R_1$  is a source,  $R_2$  is a saddle, and  $R_3$  is a sink. The system's eigenvalues and the corresponding eigenvectors associated with each finite critical point are

$$R_1: (\boldsymbol{\lambda}, \mathbf{v}) = (4.18 \times 10^7, 2.35 \times 10^7), \\ ([7.00 \times 10^{-1}, 7.14 \times 10^{-1}]^T, \\ [3.61 \times 10^{-1}, 9.33 \times 10^{-1}]^T),$$

$$R_2: (\boldsymbol{\lambda}, \mathbf{v}) = (7.11 \times 10^5, -4.64 \times 10^6), \\ ([1.00, 2.89 \times 10^{-2}]^T, \\ [-9.83 \times 10^{-1}, 1.81 \times 10^{-1}]^T),$$

$$R_3: (\boldsymbol{\lambda}, \mathbf{v}) = (-1.91 \times 10^5, -1.73 \times 10^7), \\ ([1.00, 1.79 \times 10^{-3}]^T, \\ [-1.07 \times 10^{-1}, 9.94 \times 10^{-1}]^T).$$

The eigenvalues' and eigenvectors' units are  $1/s$  and mol/g, respectively.

Since the finite root  $R_2$  has only one unstable mode, i.e., positive eigenvalue, it is a candidate point for the 1D SIM construction. Moreover, the system's physical fast and slow time scales are the ones associated with its physical equilibrium,  $R_3$ . These are, respectively,  $5.78 \times 10^{-8}$  s and  $5.24 \times 10^{-6}$  s, which give rise to a stiffness of  $\mathcal{O}(10^2)$ . So, even the two-step Zel'dovich mechanism retains stiffness at  $T = 4000$  K. The multiscale nature of this system is clearly shown in Fig. 1, where the full dynamics of the evolution of the species are presented. Here, the first reaction commences at  $t \sim 10^{-8}$  s, and the system enters its last relaxation toward the physical equilibrium state after  $t \sim 10^{-5}$  s.

## 2. Infinite equilibria

In addition to its three finite critical points, this system has equilibria at infinity. They can be identified using the projective space technique described in Sec. III C. Arbitrarily, we select  $k=1$ , so the Zel'dovich reactive system in the projective space is realized by the following transformation:  $Z_0=t, Z_1=1/z_1, Z_2=z_2/z_1$ . Subsequently, we have

$$\frac{dZ_0}{d\tau} = Z_1, \quad (37a)$$

$$\frac{dZ_1}{d\tau} = 9.98 \times 10^4 Z_1^2 - 2.51 \times 10^2 Z_1^3 + 3.22 \times 10^9 Z_1 Z_2 \\ - 1.16 \times 10^7 Z_1^2 Z_2 - 6.99 \times 10^8 Z_1 Z_2^2, \quad (37b)$$

$$\frac{dZ_2}{d\tau} = 8.47 \times 10^4 Z_1 + 2.51 \times 10^2 Z_1^2 (1 - Z_2) \\ - 1.84 \times 10^9 Z_2 - 1.16 \times 10^7 Z_1 Z_2 + 2.52 \times 10^9 Z_2^2 \\ - 1.16 \times 10^7 Z_1 Z_2^2 - 6.99 \times 10^8 Z_2^3. \quad (37c)$$

By using BERTINI to find all the  $\mathbf{Z}^e$  that satisfy  $\mathbf{F}(\mathbf{Z}^e) = 0$ , we find three equilibria,

$$I_1 \equiv (\mathbf{Z}^e) = (0, 0),$$

$$I_2 \equiv (\mathbf{Z}^e) = (0, 1.01),$$

$$I_3 \equiv (\mathbf{Z}^e) = (0, 2.60),$$

and they represent the infinite equilibria of the original system, Eq. (35). Here, all the infinite equilibria are real isolated critical points.

To investigate the dynamical character of each critical point, Eqs. (37b) and (37c) are linearized to find  $\mathbf{J}^e$ , and the eigenvalues and corresponding eigenvectors are calculated,

$$I_1: (\boldsymbol{\lambda}, \mathbf{v}) = (0, -1.84 \times 10^9), \\ ([1.00, 4.61 \times 10^{-5}]^T, [0, 1]^T),$$

$$I_2: (\boldsymbol{\lambda}, \mathbf{v}) = (2.54 \times 10^9, 1.12 \times 10^9), \\ ([1.00, -1.65 \times 10^{-2}]^T, [0, 1]^T),$$

$$I_3: (\boldsymbol{\lambda}, \mathbf{v}) = (3.65 \times 10^9, -2.90 \times 10^9), \\ ([1.00, -1.66 \times 10^{-2}]^T, [0, 1]^T),$$

where the eigenvalues' units are  $g/mol/s^2$ , the units of the first component of each eigenvector are g/mol, and the second component is dimensionless.

It is clear that  $I_2$  is a source,  $I_3$  is a saddle with one positive eigenvalue, and  $I_1$  is a nonhyperbolic critical point. Consequently, the Hartman–Grobman theorem is not applicable at  $I_1$ . The normal form theory<sup>47</sup> is utilized to investigate the dynamical character of  $I_1$ . It is found that  $I_1$  is a saddle node,<sup>49</sup> which consists of two hyperbolic sectors, one parabolic sector, and three separatrices, in the nomenclature of Ref. 41. Further details are presented in the Appendix. Only one of these separatrices is unstable. Thus,  $I_1$  and  $I_3$  are candidate points for constructing the system's 1D SIM.

## 3. The construction of the SIM

Now, following our 1D SIM construction procedure, the candidate points are ordered as follows: First  $R_2$ , second  $I_1$ , and third  $I_3$ . So, starting from the unstable direction of the candidate point  $R_2$ , Eqs. (35) are numerically integrated to generate a heteroclinic orbit. This orbit approaches  $R_3$ , the

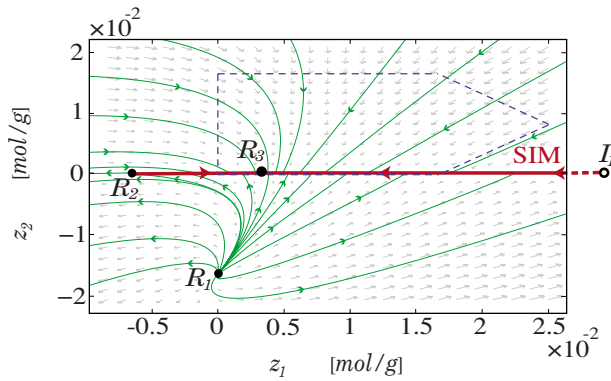


FIG. 2. A region of the finite composition space for the Zel'dovich mechanism. The solid dots represent finite critical points, the open circle represents an infinite critical point, the arrows indicate the flow directions, and the dashed simplex represents the physically accessible domain of the system,  $S$ . The SIM is illustrated as a thick line, the thin lines represent trajectories, and  $R_3$  represents the system's physical equilibrium state.

reactive system's physical equilibrium point, along its slowest mode. So, the generated orbit represents the first branch of the 1D SIM. Then, starting from the unstable direction of the candidate point  $I_1$ , Eqs. (37) are numerically integrated to generate another heteroclinic orbit. Also, this orbit approaches  $R_3$  along its slowest mode. So, it represents the second and last branch of the reactive system's 1D SIM, see Fig. 2. Subsequently, there is no need to check the third candidate point  $I_3$ .

In Fig. 2, part of the system's composition space and the SIM are shown. Upon visual examination of the attractiveness of the constructed SIM, it is clearly seen that all trajectories inside  $S$ , and some outside of it, are attracted to the constructed 1D SIM. Moreover, along the SIM's two branches, including the three equilibria  $R_3$ ,  $R_2$ , and  $I_1$ , the criteria (29) are satisfied, and  $S$  decreases monotonically along the 1D SIM; its maximum value is 0.15 at  $R_2$ .

#### 4. Relation between thermodynamics and the SIM

To examine the relationship between system's slow dynamics and thermodynamics,  $\sigma$  and  $G$  are calculated within  $S$ . In a 2D composition space, the scalar fields,  $G$  and  $\sigma$ , can be represented by contours. Near equilibrium these contours approach ellipses. The major axes of these ellipses are aligned with the eigenvector associated with the largest eigenvalue of that function's local Hessian matrix ( $\mathbf{H}$ ). Similarly, the minor axes are aligned with the eigenvector associated with the smallest eigenvalue of  $\mathbf{H}$ . Figure 3 shows several contours of the system's Gibbs free energy and irreversibility production rate along with the constructed 1D SIM for the Zel'dovich mechanism. Figure 3(a) is far from  $R_3$ , while Fig. 3(b) is an expansion in the vicinity of  $R_3$ . In Fig. 3(b) stretching has been employed to expose the difference between the contours' major/minor axes and the SIM. Even within the close neighborhood of  $R_3$  the contours' axes are not aligned with the 1D SIM. So, here equilibrium thermodynamic quantities cannot explain the 1D SIM, which describes the system's preferred path toward equilibrium. Moreover, the gradients of these thermodynamic scalar functions do not drive the system's dynamics.

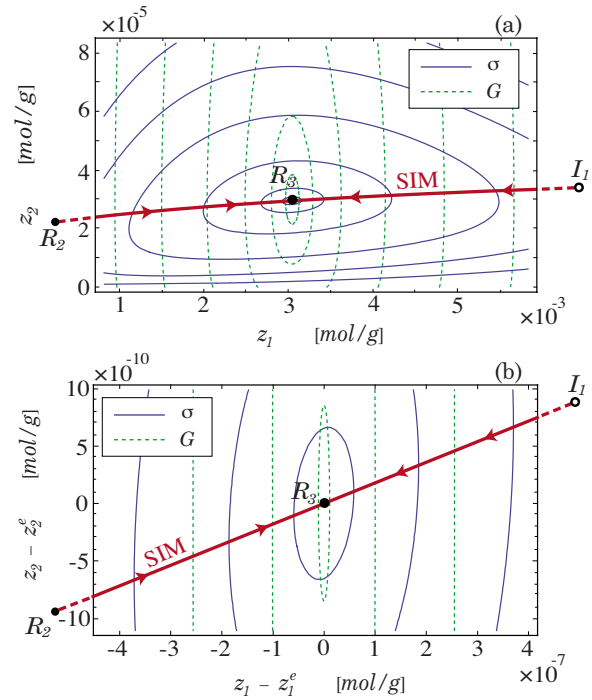


FIG. 3. (a) The SIM for the Zel'dovich mechanism near the physical equilibrium state  $R_3$ ; (b) a blow-up of the top panel in the vicinity of  $R_3$ . The solid lines and the dashed lines represent different isolevels of the system's irreversibility production rate and Gibbs free energy, respectively. The solid dots represent finite critical points, and the open circle represents an infinite critical point.

In general, in the vicinity of an equilibrium point,

$$G = G|_{z^e} + \left. \frac{\partial G}{\partial \mathbf{z}} \right|_{z=z^e} \cdot \mathbf{z}' + \frac{1}{2} \mathbf{z}'^T \cdot \mathbf{H}_G^e \cdot \mathbf{z}' + \dots, \quad (38a)$$

$$\sigma = \sigma|_{z^e} + \left. \frac{\partial \sigma}{\partial \mathbf{z}} \right|_{z=z^e} \cdot \mathbf{z}' + \frac{1}{2} \mathbf{z}'^T \cdot \mathbf{H}_\sigma^e \cdot \mathbf{z}' + \dots, \quad (38b)$$

where  $\mathbf{H}^e$  is defined as

$$H_{ij}^e = \left. \frac{\partial^2}{\partial z_i \partial z_j} \right|_{z=z^e}. \quad (38c)$$

Note that  $\mathbf{H}_G^e$  and  $\mathbf{H}_\sigma^e$  are symmetric matrices. However, the gradients of  $G$  and  $\sigma$  vanish at the physical equilibrium;  $G$  and  $\sigma$  have minima at  $\mathbf{z}^e$ . Moreover, at the equilibrium  $\sigma=0$ . So, the deviations from equilibrium values are described by

$$G - G|_{z=z^e} = \frac{1}{2} \mathbf{z}'^T \cdot \mathbf{H}_G^e \cdot \mathbf{z}' + \dots, \quad (39a)$$

$$\sigma = \frac{1}{2} \mathbf{z}'^T \cdot \mathbf{H}_\sigma^e \cdot \mathbf{z}' + \dots. \quad (39b)$$

Explicitly, for the Zel'dovich model,

$$\mathbf{H}_\sigma^e = \begin{pmatrix} 1.49 \times 10^{15} & -2.09 \times 10^{16} \\ -2.09 \times 10^{16} & 1.18 \times 10^{19} \end{pmatrix}, \quad (40a)$$

$$\mathbf{H}_G^e = \begin{pmatrix} 1.52 \times 10^{13} & -8.03 \times 10^{11} \\ -8.03 \times 10^{11} & 1.36 \times 10^{15} \end{pmatrix}, \quad (40b)$$

$$\mathbf{J}^e = \begin{pmatrix} -1.95 \times 10^5 & 1.84 \times 10^6 \\ 3.06 \times 10^4 & -1.73 \times 10^7 \end{pmatrix}. \quad (40c)$$

So, the eigenvalues and the eigenvectors of these matrices are given by

$$\mathbf{H}_G^e(\boldsymbol{\lambda}, \mathbf{v}) = (1.18 \times 10^{19}, 1.46 \times 10^{15}), \\ ([1.78 \times 10^{-3}, -1.00]^T, [-1.00, -1.78 \times 10^{-3}]^T),$$

$$\mathbf{H}_\sigma^e(\boldsymbol{\lambda}, \mathbf{v}) = (1.36 \times 10^{15}, 1.52 \times 10^{13}), \\ ([5.97 \times 10^{-4}, -1.00]^T, [-1.00, -5.97 \times 10^{-4}]^T),$$

$$\mathbf{J}^e(\boldsymbol{\lambda}, \mathbf{v}) = (-1.73 \times 10^7, -1.91 \times 10^5), \\ ([-1.07 \times 10^{-1}, 9.94 \times 10^{-1}]^T, \\ [1.00, 1.79 \times 10^{-3}]^T),$$

where for each matrix the second eigenvector yields the direction of the slow mode. It is clear that these eigenvectors are not aligned with each other. For  $\mathbf{J}^e$ , the arc tangent of the ratio between the second component and the first component of  $\mathbf{v}_2$  defines the angle  $\theta$  at which the 1D SIM approaches  $R_3$ . Similarly, the same ratio between the second component and the first component of  $\mathbf{v}_2$  of  $\mathbf{H}_G^e$  and  $\mathbf{H}_\sigma^e$  defines the angles at which each scalar field approaches  $R_3$ . These are

$$\theta_{\text{SIM}} = \tan^{-1}\left(\frac{1.79 \times 10^{-3}}{1.00}\right) = 1.79 \times 10^{-3} \text{ rad},$$

$$\theta_G = \tan^{-1}\left(\frac{-5.97 \times 10^{-4}}{-1.00}\right) = 5.97 \times 10^{-4} \text{ rad},$$

$$\theta_\sigma = \tan^{-1}\left(\frac{-1.78 \times 10^{-3}}{-1.00}\right) = 1.78 \times 10^{-3} \text{ rad}.$$

Thus, even at  $R_3$ , the reactive system's SIM cannot be identified using  $G$  or  $\sigma$ . Indeed, at  $R_3$  the error in  $\sigma$  is small; the difference between  $\theta_{\text{SIM}}$  and  $\theta_\sigma$  is  $\mathcal{O}(10^{-5})$  rad. But, this error grows as we move away from  $R_3$ . Moreover, because they are not identical, other choices of parameters would lead to larger differences.

To reinforce our point, we address this issue in more detail. Indeed, all the system's trajectories within  $S$  approach the equilibrium point in infinite time. This point is the minimum of  $G$  and  $\sigma$ . Near equilibrium, the system's dynamics relax onto the eigenvector associated with the slowest time scale. At the equilibrium point, the eigenvector associated with the smallest eigenvalue of  $\mathbf{J}^e$  defines the direction of the system's slowest mode. The major/minor axes of  $G$  and  $\sigma$  contours are aligned with the eigenvectors of  $\mathbf{H}_G^e$  and  $\mathbf{H}_\sigma^e$ , respectively. However, it is easy to show that at equilibrium there is a relationship between these two Hessians.

To find this relation, we start by substituting Eq. (16a) into Eq. (13) to obtain

$$\sigma = -\frac{M}{T} \sum_{i=1}^N \sum_{k=1}^R \bar{\mu}_i \mathcal{D}_{ik} \frac{dz_k}{dt}. \quad (41)$$

Also, by substituting Eq. (15) into Eq. (9a), we have

$$G = \sum_{i=1}^N \bar{\mu}_i \left( n_i^* + M \sum_{k=1}^R \mathcal{D}_{ik} z_k \right). \quad (42)$$

The gradient of  $G$  with respect to the reduced composition variables  $\mathbf{z}$  is given by

$$\frac{\partial G}{\partial z_k} = M \sum_{i=1}^N \bar{\mu}_i \mathcal{D}_{ik}, \quad k = 1, \dots, R. \quad (43)$$

Now, by substituting Eqs. (17a) and (43) into Eq. (41), the irreversibility production rate is given by

$$\sigma = -\frac{1}{T} \sum_{k=1}^R \frac{\partial G}{\partial z_k} \dot{w}_k. \quad (44)$$

Thus, the local Hessian of  $\sigma$  is given by

$$\frac{\partial^2 \sigma}{\partial z_i \partial z_j} = -\frac{1}{T} \sum_{k=1}^R \left( \frac{\partial G}{\partial z_k} \frac{\partial^2 \dot{w}_k}{\partial z_i \partial z_j} + \frac{\partial^2 G}{\partial z_i \partial z_k} \frac{\partial \dot{w}_k}{\partial z_j} \right. \\ \left. + \frac{\partial^2 G}{\partial z_j \partial z_k} \frac{\partial \dot{w}_k}{\partial z_i} + \frac{\partial^3 G}{\partial z_i \partial z_j \partial z_k} \dot{w}_k \right). \quad (45)$$

At equilibrium,  $G$  is minimized, and thus

$$\dot{w}_k|_{\mathbf{z}=\mathbf{z}^e} = 0, \quad k = 1, \dots, R, \quad (46a)$$

$$\frac{\partial G}{\partial z_k} \Big|_{\mathbf{z}=\mathbf{z}^e} = 0, \quad k = 1, \dots, R. \quad (46b)$$

Subsequently,

$$\frac{\partial^2 \sigma}{\partial z_i \partial z_j} \Big|_{\mathbf{z}=\mathbf{z}^e} = -\frac{1}{T} \sum_{k=1}^R \left( \frac{\partial^2 G}{\partial z_i \partial z_k} \frac{\partial \dot{w}_k}{\partial z_j} + \frac{\partial^2 G}{\partial z_j \partial z_k} \frac{\partial \dot{w}_k}{\partial z_i} \right) \Big|_{\mathbf{z}=\mathbf{z}^e}, \quad (47a)$$

or in Gibbs notation, and using Eq. (24b),

$$\mathbf{H}_\sigma^e = -\frac{1}{T} [(\mathbf{H}_G^e \cdot \mathbf{J}^e) + (\mathbf{H}_G^e \cdot \mathbf{J}^e)^T]. \quad (47b)$$

In the highly unusual case in which  $\mathbf{H}_G^e$  is diagonal with identical eigenvalues, the SIM can be identified by consideration of the eigenvectors of  $\mathbf{H}_\sigma^e$ . In that case, the eigenvectors of  $\mathbf{J}^e$  are aligned with those of  $\mathbf{H}_\sigma^e$ . However, essentially all practical reactive systems have  $\mathbf{H}_G^e$  which is not diagonal and does not have identical eigenvalues. Thus,  $\mathbf{H}_G^e$  operates on  $\mathbf{J}^e$  in a nonuniform way, such that the eigenvalues and the eigenvectors of  $\mathbf{H}_\sigma^e$  are not the same as those of  $\mathbf{J}^e$ . Thus, the system's dynamics cannot be deduced from  $\sigma$  or  $G$ . In conclusion, we can state that any approach that employs equilibrium thermodynamic potentials alone to deduce a reactive system's slow dynamics has inherent flaws.

## B. Thermodynamics-based SIM

The second example in this work is identical to the second example presented by Lebedz.<sup>19</sup> A simple closed reactive system contains three species given by the following kinetics model:  $A + A \rightleftharpoons B \rightleftharpoons C$ . Using the same argument, described in the original work,<sup>19</sup> that the total mass is conserved, the dimension of the composition space of this model

problem is reduced from  $N=3$  to  $N-1=2$ . Also, for convenience, the dimensionless variables  $c_A$  and  $c_B$  in the original work<sup>19</sup> are denoted here by  $z_1$  and  $z_2$ , respectively. The evolution of the reactive system is described by<sup>19</sup>

$$\frac{dz_1}{dt} = 10^{-5}z_2 - z_1^2, \quad (48a)$$

$$\frac{dz_2}{dt} = z_1^2 + (1 - 1002z_2 - z_1) \times 10^{-5}, \quad (48b)$$

which is in the form of Eq. (21), and it is clear that  $d=2$ .

To construct the actual SIM for this system, we use the procedure of Sec. III. For this system, two finite equilibria are found,

$$R_1 \equiv (\mathbf{z}^e) = (9.99 \times 10^{-5}, 9.99 \times 10^{-4}),$$

$$R_2 \equiv (\mathbf{z}^e) = (-1.00 \times 10^{-4}, 9.99 \times 10^{-4}).$$

The two finite equilibria are isolated points with real coordinates. Also, linear analysis in the neighborhood of each equilibrium reveals that  $R_1$  is a sink and  $R_2$  is a saddle. The eigenvalues and the associated eigenvectors at the equilibria are

$$R_1: (\boldsymbol{\lambda}, \mathbf{v}) = (-2.00 \times 10^{-4}, -1.00 \times 10^{-2}), \\ ([1.00, 1.93 \times 10^{-2}]^T, [-1.02 \times 10^{-3}, 1.00]^T),$$

$$R_2: (\boldsymbol{\lambda}, \mathbf{v}) = (2.00 \times 10^{-4}, -1.00 \times 10^{-2}), \\ ([1.00, -2.05 \times 10^{-2}]^T, [-9.79 \times 10^{-4}, 1.00]^T).$$

It is clear that  $R_1$  is the system's unique equilibrium point and  $R_2$  is a candidate saddle; its eigenvalue spectrum contains only one positive eigenvalue.

To investigate the existence of an equilibrium at infinity, the projective space technique is employed. By choosing  $k=2$ , the projective space is realized by the following transformation:  $Z_0=t, Z_1=z_1/z_2, Z_2=1/z_2$ . The reactive system's behavior at infinity is described by the following set of ODEs:

$$\frac{dZ_0}{d\tau} = Z_2, \quad (49a)$$

$$\frac{dZ_1}{d\tau} = 10^{-5}Z_2 - Z_1^2 + 10^{-5}Z_1Z_2(1002 + Z_1 - Z_2) - Z_1^3, \quad (49b)$$

$$\frac{dZ_2}{d\tau} = -Z_1^2Z_2 + 10^{-5}Z_2^2(1002 + Z_1 - Z_2). \quad (49c)$$

For this system there are two equilibria,

$$I_1 \equiv (\mathbf{Z}^e) = (0, 0),$$

$$I_2 \equiv (\mathbf{Z}^e) = (-1, 0).$$

Stability analysis in the neighborhood of these equilibria reveals that  $I_2$  is a stable proper node,<sup>41</sup> with  $\lambda_1=\lambda_2=-1$ , while  $I_1$  is a nonhyperbolic critical point with  $\lambda_1=\lambda_2=0$ . Using the normal form theory<sup>47</sup> we find that  $I_1$  is a nonhyperbolic node

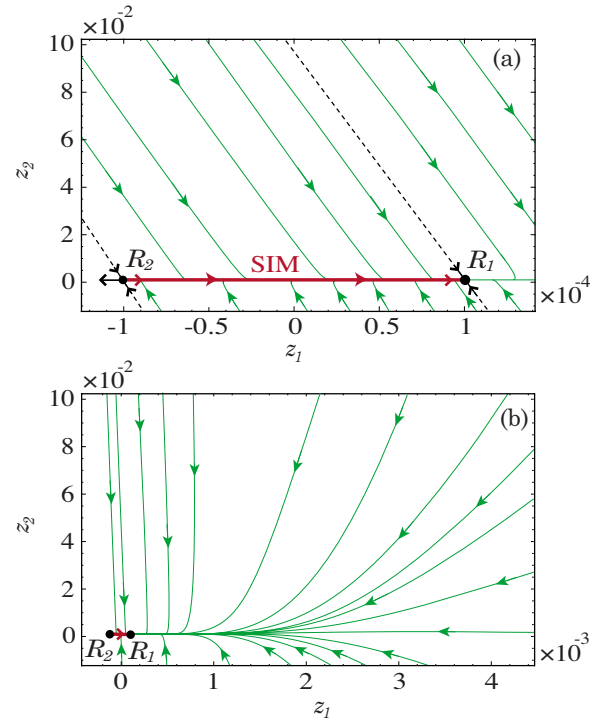


FIG. 4. Part of the finite composition space for the Lebedev system (Ref. 19). The thick line is the system's 1D SIM, the thin lines represent trajectories, the dashed lines represent the fast invariant manifolds, and the arrows indicate the flow directions.  $R_2$  is a nonphysical finite critical point and  $R_1$  represents the system's physical equilibrium point. (a) is a blow-up near the system's SIM and (b) is a wider range of the system's composition space.

which consists of two hyperbolic sectors and two parabolic sectors, in the nomenclature of Ref. 41.

Since  $R_2$  is the only critical point with one unstable direction, it is the only candidate point for this system. Consequently, the system's SIM has only one branch. In Fig. 4(a), the system's 1D SIM is presented and several trajectories have been generated away from it to examine the attractiveness of the SIM. Also, along the SIM's branches, including  $R_1$  and  $R_2$ , criteria (29) hold, and the maximum value of  $S = 1.99 \times 10^{-2}$  occurs at  $R_2$ .

Figure 4(a) shows what might be considered as a second branch for the system's 1D SIM, although our criteria indicate that this system's 1D SIM has only one branch. A wider range of the system's composition space is shown in Fig. 4(b). It is apparent that there is an attractive small region that extends horizontally to the right of  $R_1$ . However, as will be shown in Sec. IV B 1, this apparent "attractive manifold," which does not satisfy our global criteria (29), is not unique.

### 1. Global composition space

To obtain a better understanding of the dynamics of this system, sketches of the global phase portrait are illustrated in Fig. 5. Because of scaling effects, it is difficult to graphically illustrate the global dynamical behavior. First, in Fig. 5(a), the view of the projective space in the transformed coordinates is shown. Since there are two sinks for this system,  $R_1$  and  $I_2$ , there are two basins of attraction.<sup>51</sup> Each basin contains only one sink, which all the trajectories inside of it approach. The shaded area represents part of the basin of

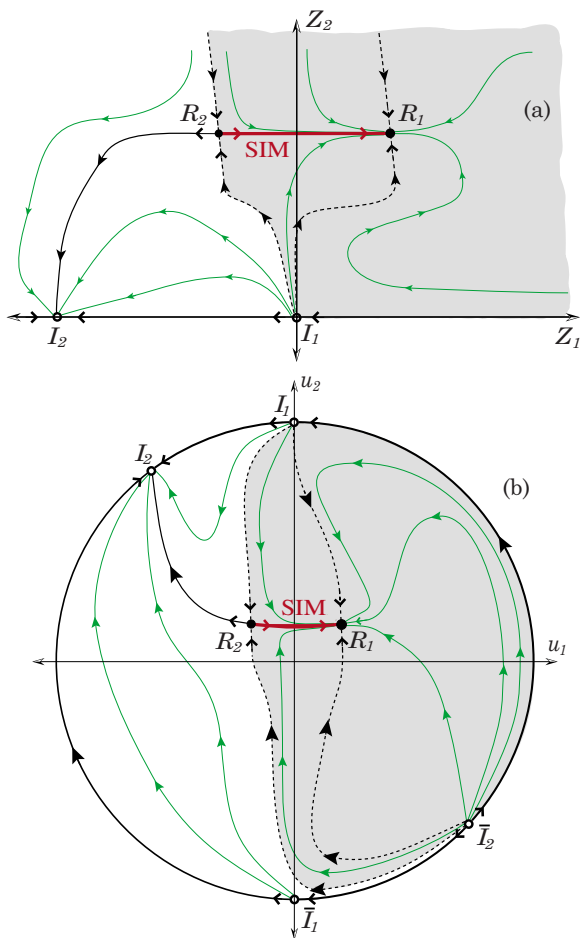


FIG. 5. Sketches of (a) the projective space portrait and (b) the global phase portrait for the Lebedez system (Ref. 19). The solid dots represent finite critical points, the shaded area represents the basin of attraction of the system's physical equilibrium state  $R_1$ , the thick line represents the SIM, the dashed lines represent the fast invariant manifolds, and the thin lines are trajectories. The open circles denote critical points at infinity and their images ( $\bar{I}_i$ ).

attraction for  $R_1$ . Also, illustrated in dashed lines, the fast invariant manifolds of  $R_2$  and  $R_1$  define the boundary between the two basins and the two parts of the basin of attraction for  $R_1$ , respectively.

Next, a projection of the system's Poincaré sphere<sup>41,52</sup> onto a 2D plane is presented in Fig. 5(b). The Poincaré sphere is a central projection technique which maps the composition space onto a sphere and is defined as

$$u_i = \frac{z_i}{\sqrt{1 + \sum_{j=1}^R z_j^2}}, \quad i = 1, \dots, R, \quad (50a)$$

$$u_{R+1} = \frac{1}{\sqrt{1 + \sum_{j=1}^R z_j^2}}. \quad (50b)$$

This technique has been used before in the literature to analyze the global dynamics of reactive systems.<sup>17,22</sup> The major disadvantage of this technique is that it is not a one-to-one transformation, although it is useful for analyzing low-dimensional systems. In Fig. 5(b), the circle's boundary represents infinity in the untransformed space and the shaded

area is the basin of attraction for  $R_1$ . Also,  $\bar{I}_1$  and  $\bar{I}_2$  are antipodal points to the infinite critical points  $I_1$  and  $I_2$ .<sup>41</sup> These antipodal points, or images, appear as a consequence of not using a one-to-one mapping, and their dynamical behavior is equivalent to  $I_1$  and  $I_2$  with reversed flow direction; i.e.,  $I_2$  is a sink and  $\bar{I}_2$  is source.

Figure 5 clearly shows that the constructed 1D SIM gives an accurate description of the asymptotic behavior of the system's trajectories, although it consists of only one branch. Moreover, it shows that the horizontal attractive submanifold near  $R_1$ , which might appear to be a second branch of the system's 1D SIM, is not unique. This apparent attractive manifold consists of heteroclinic orbits that initiate from  $\bar{I}_2$ . However, none of these orbits are attractive along their complete trajectories; near  $\bar{I}_2$  all orbits have  $S \geq 1$ .

## 2. SIM and MEPT

This system, described by Eq. (48), has been employed by Lebedez<sup>19</sup> to present the MEPT method. The MEPT method is based on minimizing a classical thermodynamic quantity, which is in this case the irreversibility production rate  $\sigma$ . To compare the system's actual 1D SIM to its MEPT, a series of calculations was performed to reproduce the MEPT. By following the same procedure described in the original work,<sup>19</sup> we were able to reconstruct the MEPT for this system. This is given by the dashed line in Fig. 6 and is identical to the one presented in Ref. 19.

Figure 6(a) is identical to Fig. 4 of Ref. 19; Fig. 6(b) shows a wider range of the system's finite composition space, and Fig. 6(c) is a closer look at the system's dynamical behavior near the physical equilibrium. Figure 6 clearly shows that the MEPT is not an attractive manifold, although near  $R_1$  it seems attractive. However, any trajectory approaching  $R_1$  from the right side is as attractive as the MEPT near  $R_1$ . Moreover, the MEPT is a subset of a heteroclinic orbit that connects  $\bar{I}_2$  with  $R_1$ , and as noted  $S \geq 1$  near  $\bar{I}_2$ . Subsequently, the MEPT is not attractive along its complete trajectory, and thus does not correspond to the SIM of the system.

## C. Simple hydrogen-oxygen reactive system

This example is adopted from Sec. II of Ren *et al.*,<sup>21</sup> where it serves as a model problem for illustrating how to construct the ICE-PIC manifold. Here, it is used to demonstrate the simplicity of extending our proposed technique to higher-dimensional reactive systems and to comment on the ICE-PIC method.

The reaction mechanism contains  $N=6$  species,  $L=3$  elements, and  $J=6$  reversible reactions, see Table II. A special case in which the system is isobaric, identical to Ren *et al.*,<sup>21</sup> will be considered. The assigned mixture temperature and pressure are  $T=3000$  K and  $p=1$  atm, respectively. The initial conditions are  $(n_1^*=3.03 \times 10^{-4}, n_2^*=1.01 \times 10^{-4}, n_3^*=3.03 \times 10^{-4}, n_4^*=2.32 \times 10^{-5}, n_5^*=1.11 \times 10^{-4}, n_6^*=3.32 \times 10^{-3})$  mol. Here,  $i=\{1,2,3,4,5,6\}$  corresponds to the species  $\{H_2, O, H_2O, H, OH, N_2\}$ , respectively. This gives rise to  $M=1.01 \times 10^{-1}$  g.

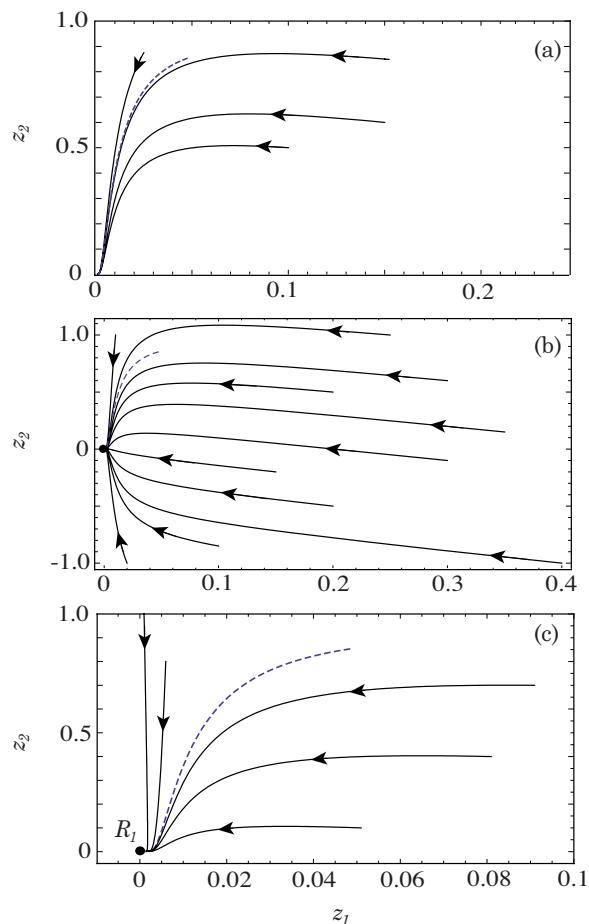


FIG. 6. The dashed line represents the calculated MEPT and the thin lines represent trajectories in the composition space of the Lebedev system (Ref. 19). (a) is identical to Fig. 4 in Ref. 19, while (b) is a wider range of the system's finite composition space, and (c) is a blowup near the system's physical equilibrium  $R_1$ . Different sets of trajectories are illustrated in each figure.

The reactive system in this model problem is described in the  $R=N-L=3$  dimensional reactive composition space. The system's only constraints are the conservation of elements; thus, the ODEs that describe the system evolution are of the form

$$\frac{d\mathbf{z}}{dt} = \mathbf{f}(\mathbf{z}), \quad \mathbf{z} \in \mathbb{R}^3. \quad (51)$$

The dynamics are fully described by  $\{\text{H}_2, \text{O}, \text{H}_2\text{O}\}$ , and the rest of the species,  $\{\text{H}, \text{OH}, \text{N}_2\}$ , are given by the system's constraints, Eq. (15),

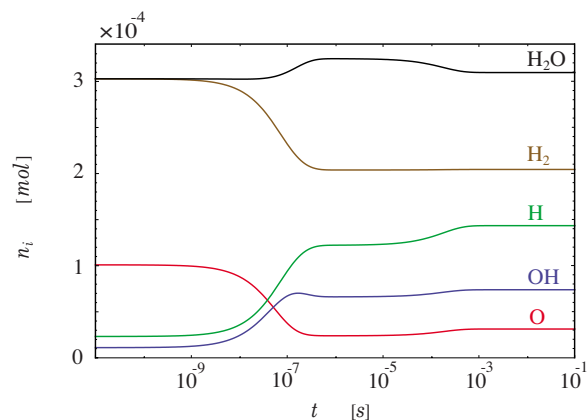


FIG. 7. The time evolution of species for the simple hydrogen-oxygen reactive system; identical to that of Ren *et al.* (Ref. 21).

$$2n_1 + 2n_3 + 2n_4 + n_5 = 1.25 \times 10^{-3} \text{ mol}, \quad (52a)$$

$$n_2 + n_3 + n_5 = 4.15 \times 10^{-4} \text{ mol}, \quad (52b)$$

$$2n_6 = 6.64 \times 10^{-3} \text{ mol}, \quad (52c)$$

which are identical to those given by Ren *et al.*<sup>21</sup>

The time evolution of the species is shown in Fig. 7. The multiscale nature of this system is clearly seen. Also, it can be noted that the times at which the first reaction event commences and that at which the system relaxes onto its equilibrium are approximately  $t=10^{-9}$  s and  $t\sim 10^{-3}$  s, respectively.

### 1. The construction of the SIM

We use the method described in Sec. III to construct the SIM for this system. First, all the system's finite equilibria are identified. There are 15 isolated critical points; eight of them are complex and seven are real. The real critical points are

$$R_1 \equiv (\mathbf{z}^e) = (-1.67 \times 10^{-1}, 3.04 \times 10^{-3}, 3.53 \times 10^{-3}) \text{ mol/g},$$

$$R_2 \equiv (\mathbf{z}^e) = (6.44 \times 10^{-2}, 1.21 \times 10^{-2}, -7.12 \times 10^{-3}) \text{ mol/g},$$

$$R_3 \equiv (\mathbf{z}^e) = (-6.47 \times 10^{-3}, -2.01 \times 10^{-2}, -2.19 \times 10^{-3}) \text{ mol/g},$$

TABLE II. Simple hydrogen-oxygen kinetics mechanism. The species are  $\text{H}_2$ ,  $\text{H}$ ,  $\text{O}$ ,  $\text{OH}$ ,  $\text{H}_2\text{O}$ , and  $\text{N}_2$ .

$j$	Reaction <sup>a</sup>	$A_j$ [(mol/cm <sup>3</sup> ) <sup>(1-\sum_{i=1}^N \nu_{ij})</sup> /s/K <sup><math>\beta_j</math></sup> ]	$\beta_j$	$\bar{E}_j$ [cal/mol]
1	$\text{O} + \text{H}_2 \rightleftharpoons \text{H} + \text{OH}$	$5.08 \times 10^4$	2.7	6 290.0
2	$\text{H}_2 + \text{OH} \rightleftharpoons \text{H}_2\text{O} + \text{H}$	$2.16 \times 10^8$	1.5	3 430.0
3	$\text{O} + \text{H}_2\text{O} \rightleftharpoons 2\text{OH}$	$2.97 \times 10^6$	2.0	13 400.0
4	$\text{H}_2 + \text{M} \rightleftharpoons 2\text{H} + \text{M}$ <sup>b</sup>	$4.58 \times 10^{19}$	-1.4	104 380.0
5	$\text{O} + \text{H} + \text{M} \rightleftharpoons \text{OH} + \text{M}$ <sup>b</sup>	$4.71 \times 10^{18}$	-1.0	0.0
6	$\text{H} + \text{OH} + \text{M} \rightleftharpoons \text{H}_2\text{O} + \text{M}$ <sup>b</sup>	$3.80 \times 10^{22}$	-2.0	0.0

<sup>a</sup>Unless otherwise specified, the third body collision efficiency coefficients are unity,  $\alpha=1$ .

<sup>b</sup>The nonunity third body collision efficiency coefficients are  $\alpha_{\text{H}_2}=2.5$  and  $\alpha_{\text{H}_2\text{O}}=12$ .

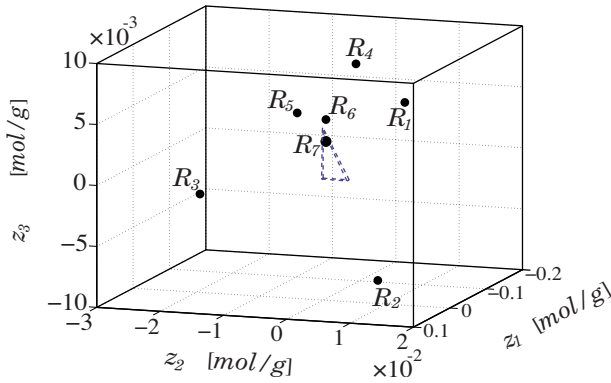


FIG. 8. A region of the finite composition space for the simple hydrogen-oxygen reactive system (Ref. 21). The dashed simplex represents the physically accessible domain of the system  $S$ , the solid dots represent finite equilibria, and the unique critical point inside the polygon,  $R_7$ , represents the physical equilibrium point.

$$R_4 \equiv (\mathbf{z}^e) = (1.98 \times 10^{-3}, 5.04 \times 10^{-3}, 9.42 \times 10^{-3}) \text{ mol/g},$$

$$R_5 \equiv (\mathbf{z}^e) = (-1.21 \times 10^{-3}, -4.45 \times 10^{-3}, 5.03 \times 10^{-3}) \text{ mol/g},$$

$$R_6 \equiv (\mathbf{z}^e) = (2.72 \times 10^{-3}, 3.34 \times 10^{-4}, 4.72 \times 10^{-3}) \text{ mol/g},$$

$$R_7 \equiv (\mathbf{z}^e) = (2.03 \times 10^{-3}, 3.10 \times 10^{-4}, 3.07 \times 10^{-3}) \text{ mol/g}.$$

It is clear that  $R_1$ ,  $R_2$ ,  $R_3$ , and  $R_5$  are nonphysical equilibria. Moreover,  $R_4$  and  $R_6$  are also nonphysical critical points; this can be shown by computing the values of other species using the system's constraints, Eq. (52). Thus,  $R_7$  is the system's unique physical equilibrium point, consistent with the results in Fig. 7.

Figure 8 shows part of the system's finite composition space, all the finite equilibria, and the system's  $S$  within the dashed simplex. The dynamical analysis within the neighborhood of each critical point reveals that  $R_3$  and  $R_7$  are sinks, and  $R_1$ ,  $R_2$ ,  $R_4$ ,  $R_5$ , and  $R_6$  are saddles. The eigenvalue spectrum associated with each finite critical point is

$$R_1: (\boldsymbol{\lambda}) = (2.92 \times 10^3, -6.67 \times 10^6 \pm i1.00 \times 10^8) \text{ s}^{-1},$$

$$R_2: (\boldsymbol{\lambda}) = (1.84 \times 10^{14}, -1.27 \times 10^{12}, -1.70 \times 10^{14}) \text{ s}^{-1},$$

$$R_3: (\boldsymbol{\lambda}) = (-1.03 \times 10^5, -2.97 \times 10^7 \pm i2.64 \times 10^7) \text{ s}^{-1},$$

$$R_4: (\boldsymbol{\lambda}) = (1.62 \times 10^7, 8.94 \times 10^6, -4.65 \times 10^4) \text{ s}^{-1},$$

$$R_5: (\boldsymbol{\lambda}) = (3.22 \times 10^4, -2.13 \times 10^6 \pm i6.71 \times 10^6) \text{ s}^{-1},$$

$$R_6: (\boldsymbol{\lambda}) = (1.57 \times 10^4, -6.28 \times 10^6 \pm i4.37 \times 10^6) \text{ s}^{-1},$$

$$R_7: (\boldsymbol{\lambda}) = (-5.59 \times 10^3, -9.08 \times 10^6, -1.77 \times 10^7) \text{ s}^{-1}.$$

The fastest and slowest time scales associated with the physical equilibrium  $R_7$  are  $5.65 \times 10^{-8}$  and  $1.79 \times 10^{-4}$  s, respec-

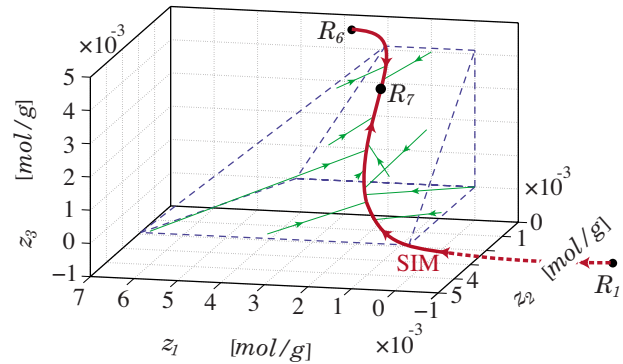


FIG. 9. The SIM for the simple hydrogen-oxygen reactive system as a thick line. The solid dots represent finite critical points,  $R_7$  represents the system's physical equilibrium state, the dashed simplex represents  $S$ , and the thin lines illustrate several trajectories.

tively. This will give rise to a stiffness  $\mathcal{O}(10^3)$ , which indicates that the system's trajectories, inside the physical domain, will relax onto the SIM at a steep angle; the fast modes will be exhausted rapidly.

To explore the existence of equilibria at infinity, the projective space technique is employed. We select  $k=2$ , although other choices would work as well. So, the reactive system in the projective space is realized by the following transformation:  $Z_0=t$ ,  $Z_1=z_1/z_2$ ,  $Z_2=1/z_2$ , and  $Z_3=z_3/z_2$ . For this system there are two equilibria located at infinity, but neither of them are isolated. One is a 1D equilibrium, and the other is a 2D equilibrium. Consequently,  $R_1$ ,  $R_2$ ,  $R_5$ , and  $R_6$  are the only candidate points, since the eigenvalue spectra of the corresponding Jacobians each contain only one unstable mode.

To construct the SIM, the dynamical system, Eq. (51), is numerically integrated, starting from the candidate points, in the direction of the unstable mode pointing toward  $R_7$ . First, we generate a heteroclinic orbit starting from  $R_1$ , since it has the slowest unstable mode among the candidate points. The generated orbit connects with  $R_7$  along its slowest mode. Thus, it represents the first branch of the system's 1D SIM. Then, we generate another heteroclinic orbit starting from  $R_6$ . This orbit also approaches  $R_7$  along its slowest mode to form the second branch of the 1D SIM. Subsequently, there is no need to generate trajectories starting from the other candidate points  $R_2$  and  $R_5$ .

The system's 1D SIM is presented in Fig. 9. Although the SIM has been constructed and it can be illustrated, the right branch of the SIM is not presented entirely due to scaling effects. Some trajectories in Fig. 9 have been generated from inside  $S$ , while others have been initiated from its boundary. The attractiveness of the SIM is revealed by visually examining the relaxation of several trajectories rapidly onto it. This observation is consistent with our previous prediction that has been obtained based on the stiffness of the system. In addition, it has been verified that along the SIM's two branches the criteria (29) hold, and the maximum value of  $S$  along the 1D SIM is approximately  $2.50 \times 10^{-3}$  at  $R_6$ . Thus, the SIM is highly attractive; this is consistent with observation and our previous prediction.

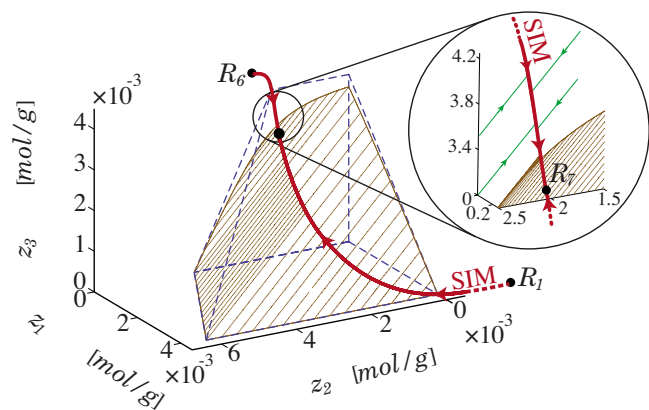


FIG. 10. A comparison between the actual 1D SIM, illustrated as thick line, and the 2D ICE manifold for the simple hydrogen-oxygen reactive system. The solid dots represent finite critical points,  $R_7$  represents the system's physical equilibrium state, and the dashed simplex represents  $S$ . Thin lines represent trajectories inside  $S$ . The ICE manifold is identical to the one presented in Ref. 21.

## 2. Comparison to ICE manifold

In this section, we compare the constructed SIM with the previously published<sup>21</sup> ICE manifold. Calculations are first performed to reproduce the ICE manifold for the considered reactive system.

Generation of the ICE manifold is based on minimizing a classical thermodynamics potential. First, the constrained equilibrium manifold (CEM) is developed by varying one dependent variable to minimize the system's Gibbs potential for each combination of the rest of the dependent variables. The intersection between the CEM and  $S$  defines a closed curve. Then, starting from several points located on the closed curve, trajectories are generated. The collection of all

these trajectories represents the ICE manifold. Figure 10 shows the 1D SIM and the 2D ICE manifold. The computed ICE manifold is identical to that illustrated in Fig. 4 of Ren et al.<sup>21</sup>

From Fig. 10, it is clear that there are trajectories within  $S$  which are not attracted to the 2D ICE manifold. However, all the system's trajectories are attracted to the 1D SIM. Although it is difficult to visualize in Fig. 10, the 2D ICE manifold does not contain the system's SIM: The 1D SIM is not a subset of the 2D ICE manifold. The error of the ICE manifold grows as we move away from  $R_7$ . Consequently, the 2D ICE manifold cannot fully identify the system's SIM.

## V. DETAILED HYDROGEN-AIR MECHANISM

In this section, the 1D SIM for a detailed hydrogen-air kinetic system is constructed. The reactive system is based on the detailed kinetic mechanism extracted from Miller et al.,<sup>53</sup> and it has been widely used in the literature.<sup>54-56</sup> This mechanism consists of  $J=19$  reversible reactions involving  $N=9$  species which are composed of  $L=3$  elements, see Table III. The system is an isochoric stoichiometric hydrogen-air mixture which is initially at  $p^*=10^7$  dyn/cm<sup>2</sup> and  $T=1500$  K.

Utilizing the conservation of the three elements  $\{H,O,N\}$ , the  $H_2$ -air reactive system can be described by the following autonomous dynamical system:

$$\frac{d\mathbf{z}}{dt} = \mathbf{f}(\mathbf{z}), \quad \mathbf{z} \in \mathbb{R}^6. \quad (53)$$

Here,  $i=\{1,2,3,4,5,6\}$  correspond to the species  $\{H_2, O_2, H, O, OH, H_2O\}$ , respectively. The rest of the species,  $\{HO_2, H_2O_2, N_2\}$ , are recast using Eq. (15).

TABLE III. Reaction mechanism rate coefficients for hydrogen-air mixture.

$j$	Reaction <sup>a</sup>	$A_j$ [(mol/cm <sup>3</sup> ) <sup>(1-\sum_{i=1}^N \nu'_{ij})</sup> /s/K <sup><math>\beta_j</math></sup> ]	$\beta_j$	$\bar{E}_j$ [cal/mol]
1	$H_2 + O_2 \rightleftharpoons 2OH$	$1.70 \times 10^{13}$	0.000	47 780
2	$OH + H_2 \rightleftharpoons H_2O + H$	$1.17 \times 10^9$	1.300	3626
3	$H + O_2 \rightleftharpoons OH + O$	$5.13 \times 10^{16}$	-0.816	16 507
4	$O + H_2 \rightleftharpoons OH + H$	$1.80 \times 10^{10}$	1.000	8826
5	$H + O_2 + M \rightleftharpoons HO_2 + M$ <sup>b</sup>	$2.10 \times 10^{18}$	-1.000	0
6	$H + 2O_2 \rightleftharpoons HO_2 + O_2$	$6.70 \times 10^{19}$	-1.420	0
7	$H + O_2 + N_2 \rightleftharpoons HO_2 + N_2$	$6.70 \times 10^{19}$	-1.420	0
8	$OH + HO_2 \rightleftharpoons H_2O + O_2$	$5.00 \times 10^{13}$	0.000	1000
9	$H + HO_2 \rightleftharpoons 2OH$	$2.50 \times 10^{14}$	0.000	1900
10	$O + HO_2 \rightleftharpoons O_2 + OH$	$4.80 \times 10^{13}$	0.000	1000
11	$2OH \rightleftharpoons O + H_2O$	$6.00 \times 10^8$	1.300	0
12	$H_2 + M \rightleftharpoons 2H + M$ <sup>c</sup>	$2.23 \times 10^{12}$	0.500	92 600
13	$O_2 + M \rightleftharpoons 2O + M$	$1.85 \times 10^{11}$	0.500	95 560
14	$H + OH + M \rightleftharpoons H_2O + M$ <sup>d</sup>	$7.50 \times 10^{23}$	-2.600	0
15	$H + HO_2 \rightleftharpoons H_2 + O_2$	$2.50 \times 10^{13}$	0.000	700
16	$2HO_2 \rightleftharpoons H_2O_2 + O_2$	$2.00 \times 10^{12}$	0.000	0
17	$H_2O_2 + M \rightleftharpoons 2OH + M$	$1.30 \times 10^{17}$	0.000	45 500
18	$H_2O_2 + H \rightleftharpoons HO_2 + H_2$	$1.60 \times 10^{12}$	0.000	3800
19	$H_2O_2 + OH \rightleftharpoons H_2O + HO_2$	$1.00 \times 10^{13}$	0.000	1800

<sup>a</sup>Unless otherwise specified, the third body collision efficiency coefficients are unity,  $\alpha=1$ .

<sup>b</sup>The nonunity third body collision efficiency coefficients are  $\alpha_{H_2}=3.3$  and  $\alpha_{H_2O}=21$ .

<sup>c</sup>The nonunity third body collision efficiency coefficients are  $\alpha_{H_2}=3$ ,  $\alpha_{H_2O}=6$ , and  $\alpha_H=2$ .

<sup>d</sup>The nonunity third body collision efficiency coefficients are  $\alpha_{H_2O}=20$ .

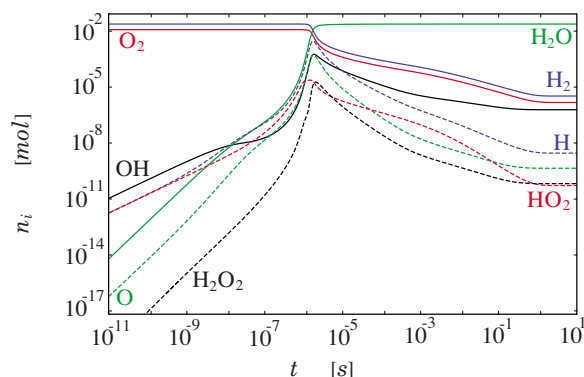


FIG. 11. The time evolution of species for the hydrogen-air reactive system.

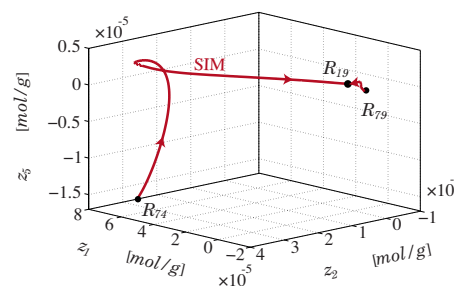
The full dynamics of the species evolution are obtained by integrating Eq. (53), see Fig. 11. At  $t \approx 10^{-8}$  s, the species growth rates change slightly, which indicates that significant dissociation reactions are induced. For  $10^{-7} < t < 10^{-6}$  s, the minor species continue to increase rapidly with different growth rates. On the other hand, the major species  $H_2$ ,  $O_2$ , and  $N_2$  have essentially constant specific moles. Just past  $t \approx 10^{-6}$  s all the species undergo significant change, and the radicals' specific moles reach their maximum values. At  $t \approx 10^{-5}$  s, an exothermic recombination of radicals commences forming the predominant product  $H_2O$ , which continues up to  $t \approx 5$  s, after which the system approaches the equilibrium state. Figure 11 clearly illustrates the multiscale nature of this system.

The first step in constructing the SIM, following the methodology presented in Sec. III, is to find all of the system's real isolated equilibria, finite and infinite. For this system 284 finite equilibria and 42 infinite equilibria are found. Of the finite equilibria, 1 is 3D, 1 is 2D, 6 are 1D, and 276 are zero dimensional (0D). Of the 276 0D equilibria, 90 are real, and 186 are complex. Of the 42 infinite equilibria, 6 are 1D and 36 are 0D. Of the latter 0D equilibria, 18 are complex and 18 are real. One of the 90 real finite critical points represents the unique physical equilibrium state of the system. This corresponds to

$$R_{19} \equiv (\mathbf{z}^e) = (1.98 \times 10^{-6}, 9.00 \times 10^{-7}, 1.72 \times 10^{-9}, 2.67 \times 10^{-10}, 3.66 \times 10^{-7}, 1.44 \times 10^{-2}) \text{ mol/g.}$$

Then, the dynamical character of each of the 108 isolated real finite and infinite critical points is determined. It is found that among them there are only 14 candidate points for constructing the SIM; all of them are finite. The other critical points are either sources, sinks, or saddles with more than one unstable direction. By examining the trajectories that emanate from the candidate points, only two are connected with  $R_{19}$  tangent to its slowest mode via heteroclinic orbits. These two candidate points are

$$R_{74} \equiv (\mathbf{z}^e) = (6.26 \times 10^{-5}, 3.43 \times 10^{-5}, -2.30 \times 10^{-6}, 4.80 \times 10^{-7}, -1.54 \times 10^{-5}, 1.44 \times 10^{-2}) \text{ mol/g,}$$

FIG. 12. The 1D SIM for the detailed  $H_2$ -air mechanism. The solid dots represent finite critical points and  $R_{19}$  represents the system's physical equilibrium state.

$$R_{79} \equiv (\mathbf{z}^e) = (-3.34 \times 10^{-6}, -1.50 \times 10^{-6}, 5.27 \times 10^{-9}, 8.82 \times 10^{-10}, -6.66 \times 10^{-7}, 1.44 \times 10^{-2}) \text{ mol/g,}$$

and these two heteroclinic orbits combine to provide the two branches of the 1D SIM. Figure 12 shows a 3D projection of the 1D SIM embedded inside the six-dimensional composition space. The 1D SIM is attractive along the complete trajectories; criteria (29) hold along the SIM's branches. Subsequently, it provides the best description of the system's slow dynamics.

## VI. CONCLUSIONS

We have presented a robust method of constructing a 1D SIM for a closed, spatially homogenous, isothermal, reactive system described by detailed kinetics. The SIM corresponds to the exact description of the slow dynamics in the composition space of the reactive system. The construction method is based on a geometrical approach that relies upon finding and examining the dynamical behavior of all of the system's critical points. It has been shown that the construction of a 1D SIM is algorithmically easy and computationally efficient. The resulting procedure provides a useful tool to significantly reduce the computational cost associated with modeling reactive systems. The extension to nonisothermal reactive systems and higher-dimensional SIMs will be addressed in the future.

We have investigated the relationship between thermodynamics and a reactive system's SIM. It has been demonstrated that a reactive system's 1D SIM cannot be identified by consideration of the topology of a classical thermodynamic function, such as  $\sigma$ ,  $S$ , or  $G$ , even near the equilibrium state. This point has been confirmed by a mathematical proof which shows that equilibrium thermodynamic potentials do not alone determine reactive systems' dynamics during their approach toward the physical equilibrium.

## ACKNOWLEDGMENTS

The authors recognize the support of the National Science Foundation (NSF) under Grant No. CBET-0650843 and the Center for Applied Mathematics at the University of Notre Dame. A.J.S. and J.D.H. acknowledge the support of the Duncan Chair of the University of Notre Dame and the NSF under Grant Nos. DMS-0410047 and DMS-0712910. In

addition, J.A.D. is supported by NSF Grant No. DMS-0653678. The authors also appreciate the useful comments of the referees.

## APPENDIX: ELEMENTS OF DYNAMICAL SYSTEMS THEORY

In this appendix, we briefly describe the Hartman–Grobman theorem, the normal form theory, and the following terms: A hyperbolic equilibrium point, a dynamical system separatrix, a parabolic sector, and a hyperbolic sector.<sup>41,47,49</sup>

Consider a standard nonlinear dynamical system described by

$$\frac{dz}{dt} = \mathbf{f}(z), \quad z \in \mathbb{R}^R. \quad (\text{A1})$$

A point  $z^e$  is called an equilibrium point of the system if  $\mathbf{f}(z^e) = \mathbf{0}$ . Now  $\mathbf{f}(z)$  can be linearized in the neighborhood of  $z^e$ ,

$$\mathbf{f}(z) = \mathbf{J}^e \cdot (z - z^e) + \frac{1}{2}(z - z^e)^T \cdot \mathbf{H}^e \cdot (z - z^e) + \cdots, \quad (\text{A2})$$

where  $\mathbf{J}^e$  and  $\mathbf{H}^e$  are the local Jacobian and Hessian matrices, respectively, evaluated at  $z^e$ . For this dynamical system, we have the following.

- (1) The point  $z^e$  is a hyperbolic equilibrium point of the system, if none of the eigenvalues of  $\mathbf{J}^e$  evaluated at  $z^e$  has zero real part. Otherwise,  $z^e$  is a nonhyperbolic equilibrium point of the system.
- (2) A sector in the composition space of this system is an open region in the neighborhood of any  $z^e$ . Any sector is one of three types: elliptic, parabolic, or hyperbolic. If the trajectories within the sector are homoclinic orbits, it is an elliptic sector. If the trajectories within the sector are heteroclinic orbits that connect  $z^e$  with another equilibrium point, it is a parabolic sector. Otherwise, it is a hyperbolic sector.
- (3) The trajectories that represent the boundaries of a hyperbolic sector are called separatrices. These separatrices approach  $z^e$  as  $t \rightarrow \pm \infty$ .

The Hartman–Grobman theorem is used to identify the local behavior of standard dynamical systems in the neighborhood of its hyperbolic equilibria. Basically, if Eq. (A1) has a hyperbolic equilibrium point  $z^e$ , then the theorem states that the local behavior of the dynamical system in the vicinity of  $z^e$  is qualitatively the same as the behavior of the following linear system:

$$\frac{dz}{dt} = \mathbf{J}^e \cdot (z - z^e). \quad (\text{A3})$$

In other words, the local behavior of the dynamical system in the vicinity of  $z^e$  is approximated by the leading term of its Taylor's series.

On the other hand, the normal form theory is used to identify the local behavior of a standard dynamical system in the neighborhood of a nonhyperbolic equilibrium point. Basically, a local nonlinear coordinate transformation is constructed so that the nonlinear part of the original dynamical system is brought to a canonical form.

- <sup>1</sup>J. H. Seinfeld and S. N. Pandis, *Atmospheric Chemistry and Physics: From Air Pollution to Climate Change* (Wiley, New York, 1998).
- <sup>2</sup>A. L. Kuharsky and A. L. Fogelson, *Biophys. J.* **80**, 1050 (2001).
- <sup>3</sup>J. F. Griffiths, *Prog. Energy Combust. Sci.* **21**, 25 (1995).
- <sup>4</sup>J. M. Powers, *J. Propul. Power* **22**, 1217 (2006).
- <sup>5</sup>Z. Ren and S. B. Pope, *Combust. Flame* **147**, 243 (2006).
- <sup>6</sup>T. Turanyi, T. Berces, and S. Vajda, *Int. J. Chem. Kinet.* **21**, 83 (1989).
- <sup>7</sup>G. Li, A. Tomlin, H. Rabitz, and J. Toth, *J. Chem. Phys.* **101**, 1172 (1994).
- <sup>8</sup>L. Petzold and W. Zhu, *AIChE J.* **45**, 869 (1999).
- <sup>9</sup>T. Lu and C. K. Law, *Proc. Combust. Inst.* **30**, 1333 (2005).
- <sup>10</sup>U. Maas and S. B. Pope, *Combust. Flame* **88**, 239 (1992).
- <sup>11</sup>V. Bykov, V. Gol'dshtein, and U. Maas, *Combust. Theory Modell.* **12**, 389 (2008).
- <sup>12</sup>S. H. Lam and D. A. Goussis, *Proc. Combust. Inst.* **22**, 931 (1988).
- <sup>13</sup>S. H. Lam, *Combust. Sci. Technol.* **89**, 375 (1993).
- <sup>14</sup>S. H. Lam and D. A. Goussis, *Int. J. Chem. Kinet.* **26**, 461 (1994).
- <sup>15</sup>M. R. Roussel and S. J. Fraser, *J. Chem. Phys.* **93**, 1072 (1990).
- <sup>16</sup>M. R. Roussel and S. J. Fraser, *J. Chem. Phys.* **94**, 7106 (1991).
- <sup>17</sup>M. J. Davis and R. T. Skodje, *J. Chem. Phys.* **111**, 859 (1999).
- <sup>18</sup>A. N. Gorban, I. V. Karlin, and A. Y. Zinovyev, *Phys. Rep.* **396**, 197 (2004).
- <sup>19</sup>D. Lebedez, *J. Chem. Phys.* **120**, 6890 (2004).
- <sup>20</sup>A. N. Gorban and I. V. Karlin, *Chem. Eng. Sci.* **58**, 4751 (2003).
- <sup>21</sup>Z. Ren, S. B. Pope, A. Vladimirovsky, and J. M. Guckenheimer, *J. Chem. Phys.* **124**, 114111 (2006).
- <sup>22</sup>F. Creta, A. Adrover, S. Cerbelli, M. Valorani, and M. Giona, *J. Phys. Chem. A* **110**, 13447 (2006).
- <sup>23</sup>F. Creta, A. Adrover, S. Cerbelli, M. Valorani, and M. Giona, *J. Phys. Chem. A* **110**, 13463 (2006).
- <sup>24</sup>A. Zagaris, H. G. Kaper, and T. J. Kaper, *J. Nonlinear Sci.* **14**, 59 (2004).
- <sup>25</sup>D. A. Goussis, M. Valorani, F. Creta, and H. N. Najm, *Prog. Comput. Fluid Dyn.* **5**, 316 (2005).
- <sup>26</sup>S. Singh, J. M. Powers, and S. Paolucci, *J. Chem. Phys.* **117**, 1482 (2002).
- <sup>27</sup>J. Warnatz, U. Maas, and R. W. Dibble, *Combustion* (Springer, Berlin, 1999).
- <sup>28</sup>V. Reinhardt, M. Winckler, and D. Lebedez, *J. Phys. Chem. A* **112**, 1712 (2008).
- <sup>29</sup>J. C. Keck and D. Gillespie, *Combust. Flame* **17**, 237 (1971).
- <sup>30</sup>S. Ugarte, Y. Gao, and H. Metghalchi, *Int. J. Thermodyn.* **8**, 43 (2005).
- <sup>31</sup>Z. Ren, S. B. Pope, A. Vladimirovsky, J. M. Guckenheimer, and M. John, *Proc. Combust. Inst.* **31**, 473 (2007).
- <sup>32</sup>H. G. Kaper and T. J. Kaper, *Physica D* **165**, 66 (2002).
- <sup>33</sup>M. Valorani, F. Creta, D. A. Goussis, J. C. Lee, and H. N. Najm, *Combust. Flame* **146**, 29 (2006).
- <sup>34</sup>S. R. de Groot and P. Mazur, *Non-Equilibrium Thermodynamics* (Dover, New York, 1984).
- <sup>35</sup>I. Müller and W. Weiss, *Entropy and Energy: A Universal Competition* (Springer, Berlin, 2005).
- <sup>36</sup>I. Prigogine and R. Defay, *Chemical Thermodynamics* (Longmans, London, 1954).
- <sup>37</sup>W. J. Vincenti and C. H. Kruger, *Introduction to Physical Gas Dynamics* (Wiley, New York, 1965).
- <sup>38</sup>H. B. Callen, *Thermodynamics and an Introduction to Thermostatistics* (Wiley, New York, 1985).
- <sup>39</sup>I. Prigogine, *Introduction to Thermodynamics of Irreversible Processes* (Interscience, New York, 1967).
- <sup>40</sup>J. M. Powers and S. Paolucci, *Am. J. Phys.* **76**, 848 (2008).
- <sup>41</sup>L. Perko, *Differential Equations and Dynamical Systems* (Springer, New York, 2001).
- <sup>42</sup>A. J. Sommese and C. W. Wampler, *The Numerical Solution of Systems of Polynomials Arising in Engineering and Science* (World Scientific, Hackensack, NJ, 2005).
- <sup>43</sup>S. J. Fraser, *J. Chem. Phys.* **116**, 1277 (2002).
- <sup>44</sup>D. J. Bates, J. D. Hauenstein, A. J. Sommese, and C. W. Wampler, *BERTINI*, software for numerical algebraic geometry, available at <http://www.nd.edu/~sommese/bertini>.
- <sup>45</sup>R. J. Kee, F. M. Rupley, and J. A. Miller, Sandia National Laboratories Report No. SAND87-8215B, 1992.
- <sup>46</sup>A. Morgan, *Solving Polynomial Systems Using Continuation for Engineering and Scientific Problems* (Prentice Hall, Englewood Cliffs, NJ, 1987).
- <sup>47</sup>J. Guckenheimer and P. Holmes, *Nonlinear Oscillation, Dynamical Sys-*

- tems, and Bifurcations of Vector Fields* (Springer-Verlag, New York, 1983).
- <sup>48</sup>D. B. Shear, *J. Chem. Phys.* **48**, 4144 (1968).
- <sup>49</sup>A. A. Andronov, *Qualitative Theory of Second Order Dynamical Systems* (Wiley, New York, 1973).
- <sup>50</sup>D. L. Baulch, C. T. Bowman, C. J. Cobos, R. A. Cox, T. Just, J. A. Kerr, M. J. Pilling, D. Stocker, J. Troe, W. Tsang, R. W. Walker, and J. Warnatz, *J. Phys. Chem. Ref. Data* **34**, 757 (2005).
- <sup>51</sup>A. J. Lichtenberg and M. A. Leiberman, *Regular and Chaotic Dynamics* (Springer-Verlag, New York, 1992).
- <sup>52</sup>S. Lefschetz, *Differential Equations: Geometric Theory* (Interscience, New York, 1963).
- <sup>53</sup>J. A. Miller, R. E. Mitchell, M. D. Smooke, and R. J. Kee, *Proc. Combust. Inst.* **19**, 181 (1982).
- <sup>54</sup>M. D. Smooke, J. A. Miller, and R. J. Kee, *Combust. Sci. Technol.* **34**, 79 (1983).
- <sup>55</sup>F. Dabireau, B. Cuenot, O. Vermorel, and T. Poinso, *Combust. Flame* **135**, 123 (2003).
- <sup>56</sup>J. M. Powers and S. Paolucci, *AIAA J.* **43**, 1088 (2005).